Journal of Volcanology and Geothermal Research 259 (2013) 290–307

Contents lists available at SciVerse ScienceDirect

Journal of Volcanology and Geothermal Research

journal homepage: www.elsevier.com/locate/jvolgeores

Evaluation of Redoubt Volcano's sulfur dioxide emissions by the Ozone Monitoring Instrument

Taryn Lopez [a,b,*], Simon Carn [c], Cynthia Werner [d], David Fee [e], Peter Kelly [f], Michael Doukas [f], Melissa Pfeffer [g], Peter Webley [a], Catherine Cahill [a,b], David Schneider [d]

[a] Alaska Volcano Observatory, Geophysical Institute, University of Alaska Fairbanks, 903 Koyukuk Drive, Fairbanks, AK 99775, USA
[b] Department of Chemistry and Biochemistry, University of Alaska Fairbanks, 900 Yukon Drive, Fairbanks, AK 99775, USA
[c] Department of Geological and Mining Engineering and Sciences, Michigan Technological University, 1400 Townsend Drive, Houghton, MI 49931, USA
[d] U.S. Geological Survey Alaska Volcano Observatory, 4200 University Drive, Anchorage, AK 99508, USA
[e] Wilson Infrasound Observatories, Geophysical Institute, University of Alaska Fairbanks, 903 Koyukuk Drive, Fairbanks, AK 99775, USA
[f] U.S. Geological Survey Cascades Volcano Observatory, 1300 SE Cardinal Ct #100, Vancouver, WA 98683, USA
[g] Department of Geosciences, University of Oslo, P.O. Box 1047, Blindern 0316, Oslo, Norway

ARTICLE INFO

Article history:
Received 2 June 2011
Accepted 14 March 2012
Available online 23 March 2012

Keywords:
Sulfur dioxide
Redoubt Volcano
Ozone Monitoring Instrument
Remote sensing
Volcanic gases

ABSTRACT

The 2009 eruption of Redoubt Volcano, Alaska, provided a rare opportunity to compare satellite measurements of sulfur dioxide (SO_2) by the Ozone Monitoring Instrument (OMI) with airborne SO_2 measurements by the Alaska Volcano Observatory (AVO). Herein we: (1) compare OMI and airborne SO_2 column density values for Redoubt's tropospheric plume, (2) calculate daily SO_2 masses from Mount Redoubt for the first three months of the eruption, (3) develop simple methods to convert daily measured SO_2 masses into emission rates to allow satellite data to be directly integrated with the airborne SO_2 emissions dataset, (4) calculate cumulative SO_2 emissions from the eruption, and (5) evaluate OMI as a monitoring tool for high-latitude degassing volcanoes. A linear correlation (R^2 ~ 0.75) is observed between OMI and airborne SO_2 column densities. OMI daily SO_2 masses for the sample period ranged from ~60.1 kt on 24 March to below detection limit, with an average daily SO_2 mass of ~6.7 kt. The highest SO_2 emissions were observed during the initial part of the explosive phase and the emissions exhibited an overall decreasing trend with time. OMI SO_2 emission rates were derived using three methods and compared to airborne measurements. This comparison yields a linear correlation (R^2 ~ 0.82) with OMI-derived emission rates consistently lower than airborne measurements. The comparison results suggest that OMI's detection limit for high latitude, springtime conditions varies from ~2000 to 4000 t/d. Cumulative SO_2 masses calculated from daily OMI data for the sample period are estimated to range from 542 to 615 kt, with approximately half of this SO_2 produced during the explosive phase of the eruption. These cumulative masses are similar in magnitude to those estimated for the 1989–90 Redoubt eruption. Strong correlations between daily OMI SO_2 mass and both tephra mass and acoustic energy during the explosive phase of the eruption suggest that OMI data may be used to infer relative eruption size and explosivity. Further, when used in conjunction with complementary datasets, OMI daily SO_2 masses may be used to help distinguish explosive from effusive activity and identify changes in lava extrusion rates. The results of this study suggest that OMI is a useful volcano monitoring tool to complement airborne measurements, capture explosive SO_2 emissions, and provide high temporal resolution SO_2 emissions data that can be used with interdisciplinary datasets to illuminate volcanic processes.

1. Introduction

Measurements of volcanic sulfur dioxide (SO_2) emissions provide useful information for volcano monitoring and hazard mitigation. Changes in SO_2 emissions frequently precede volcanic eruptions (Daag et al., 1996; McGee et al., 2010) and can indicate processes such as the influx of new magma (Daag et al., 1996), conduit sealing (Fischer et al., 1996; Carn et al., 2008a), or scrubbing by hydrothermal waters (Symonds et al., 2001). Thus regular monitoring of volcanic SO_2 emissions may facilitate more accurate eruption forecasting. Recent advancements in detection capabilities of satellite sensors allow lower magnitude SO_2 emissions to be detected than was previously possible from space (Carn et al., 2007, 2008b). Hence satellite sensors are now able to detect non-eruptive SO_2 emissions, allowing space-based monitoring of volcanic degassing (Carn et al., 2008b). Continual satellite SO_2 measurements have recently been used to

* Corresponding author at: Alaska Volcano Observatory, Geophysical Institute, University of Alaska Fairbanks, 903 Koyukuk Drive, Fairbanks, AK 99775, USA. Tel.: +1 907 474 5713; fax: +1 907 474 5618.
E-mail address: tlopez@gi.alaska.edu (T. Lopez).

0377-0273
doi:10.1016/j.jvolgeores.2012.03.002

identify periods of open-system degassing and conduit sealing at Galeras Volcano, Colombia and Reventador Volcano, Ecuador (Carn et al., 2008a); and when used in conjunction with complementary geophysical datasets, helped forecast an impending paroxysmal eruption of Merapi Volcano, Indonesia (Surono et al., 2012). Additionally, volcanic eruption clouds frequently contain ash in addition to SO_2 (and other volatile species), and thus satellite-based detection of SO_2 emissions can in cases be used to track volcanic ash clouds and potentially help mitigate ash-aviation hazards when traditional ash-detection methods are not applicable (Carn et al., 2009; Thomas and Prata, 2011).

The Alaska Volcano Observatory (AVO) is responsible for monitoring over 50 historically active volcanoes (Schaefer et al., 2009) and providing warnings of volcanic ash clouds present in North Pacific airspace in cooperation with the National Weather Service (NWS) and the Federal Aviation Administration (FAA) (Neal et al., 2010). The traditional method employed by AVO for monitoring volcanic gases is through airborne surveys in which below-plume measurements of SO_2 column density are collected using an ultraviolet (UV) Correlation Spectrometer (COSPEC) (Doukas and McGee, 2007; McGee et al., 2010; Werner et al., 2011). More recently, in situ measurements of CO_2, SO_2, H_2S, and O_3 have been collected by flying contoured traverses within the plume (Doukas and McGee, 2007; McGee et al., 2010; Kelly et al., 2013; Werner et al., 2013). During periods of quiescence, airborne gas surveys are conducted once or twice per year at more than eight active volcanoes located within ~450 km of Anchorage, Alaska (Fig. 1). During volcanic unrest airborne surveys are conducted more frequently, sometimes as many as two or more per week. Weather restrictions and the cost associated with airborne surveys prevent more frequent measurements at many Alaskan volcanoes, even during unrest. At present, less than half of Alaska's historically active volcanoes are monitored by AVO using onsite instrumentation (including seismometers, GPS stations, web-cameras, etc.). The large number of remote and unmonitored volcanoes, combined with the challenges of obtaining high temporal resolution gas measurements, makes satellite remote sensing of SO_2 emissions a potentially significant monitoring tool. However, in order for satellite SO_2 measurements to be used for volcano monitoring, the data must first be validated and made comparable to standard airborne gas measurements.

The 2009 eruption of Redoubt Volcano, Alaska (60.4852°N, 152.7438°W, 3108 m; Fig. 1) provided a rare opportunity to validate satellite measurements of volcanic SO_2 for two reasons: (1) Mount Redoubt produced elevated SO_2 emissions that were detected by the UV Ozone Monitoring Instrument (OMI) on NASA's Aura satellite on a near-daily basis for the three months following the eruption onset, and (2) Mount Redoubt's close proximity to Anchorage (~166 km) enabled AVO scientists to collect airborne measurements of SO_2 on 11 days during this time period that could be compared with the OMI SO_2 data.

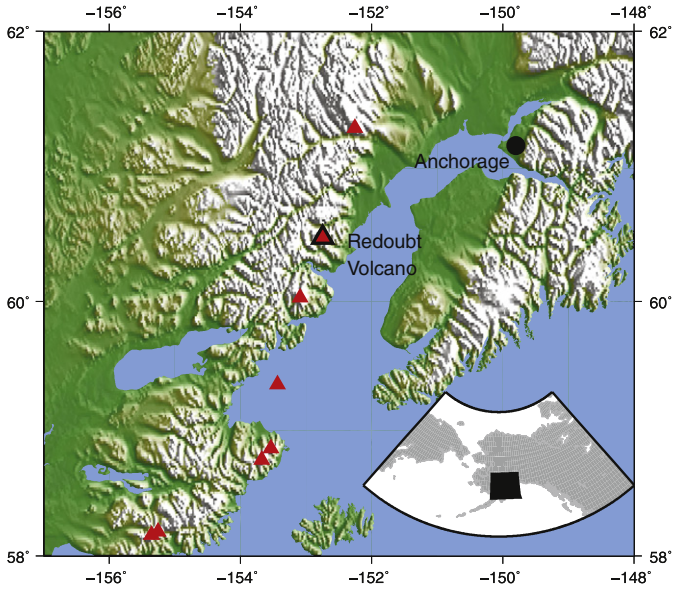

Fig. 1. Map depicting location of Redoubt Volcano and other volcanoes (black triangles) within Alaska's Cook Inlet. Anchorage, the largest population center in Alaska is labeled.

In this manuscript we compare SO_2 emissions detected by OMI with contemporaneous airborne gas measurements by: (1) developing a method to enable the OMI and airborne SO_2 column density measurements to be compared accounting for their different spatial resolution (Section 3.4), (2) calculating daily OMI measured SO_2 masses from Redoubt (Section 3.5), and (3) developing and testing methods to convert daily OMI SO_2 mass into emission rate to allow the OMI data to be directly integrated into existing emissions datasets (Section 3.6). We then use the OMI SO_2 data to estimate cumulative SO_2 emissions throughout the 2009 eruption, compare these values to Mount Redoubt's 1989–1990 eruption, and propose correlations between SO_2 emissions and Redoubt Volcano's 2009 eruptive activity (Sections 4.6, 5.6 and 5.7). Finally, we evaluate OMI as a volcano monitoring tool that can be used to increase volcanic emissions datasets, and improve the monitoring capabilities of AVO and other volcano observatories worldwide (Section 5.9).

2. Background

2.1. Overview of the 2009 eruption of Redoubt Volcano

The first observations of unrest leading up to the 2009 eruption of Redoubt Volcano occurred late in July 2008 when AVO geologists conducting fieldwork on Mount Redoubt's edifice smelled H_2S gas (Schaefer et al., 2012), though retrospective analysis found ground deformation signals as early as May 2008 (Grapenthin et al., 2013). Melting of summit ice (Bleick et al., 2013), elevated CO_2 emissions (Werner et al., 2013) and increased seismicity (Buurman et al., 2013) were all observed throughout the fall and winter of 2008. Further increases in seismicity (Buurman et al., 2013), gas emissions (Werner et al., 2013), and ice-melt (Bleick et al., 2013) were observed throughout January and February 2009. On 15 March a small phreatic explosion occurred that deposited ash on Mount Redoubt's summit and was associated with elevated gas emissions (Schaefer et al., 2012). On 20 March a seismic swarm began that lasted for 66 h (Buurman et al., 2013). In the final hours of the swarm, satellite data indicated that extrusion of a lava dome occurred (Bull and Buurman, 2013). At 6:34 (UTC) on 23 March 2009 the first in a series of magmatic explosions that comprised the explosive phase of Mount Redoubt's eruption (23 March through 4 April 2009) occurred. This phase of the eruption consisted of 19 discrete explosive magmatic eruptions (Schaefer et al., 2012; Bull and Buurman, 2013), many of which produced: ash clouds to stratospheric altitudes (Schneider and Hoblitt, 2013), elevated SO_2 emissions (this study; Werner et al., 2013), significant infrasound energy (Fee et al., 2013), ash fall (Wallace et al., 2013), pyroclastic flows (Schaefer et al., 2012; Bull and Buurman, 2013), and lahars (Schaefer et al., 2012; Bull and Buurman, 2013). Intermittent dome growth and collapse also occurred throughout this phase (Bull and Buurman, 2013). A detailed chronology of the explosive phase can be found in Table 1. Following the final explosive eruption (Event 19) on 4 April, activity at Redoubt Volcano became effusive in nature, as the final lava dome of the eruption began to grow in the summit crater (Bull and Buurman, 2013). Dome growth was associated with elevated gas emissions that decreased throughout the course of the eruption (Werner et al., 2013). Lava effusion continued through 1 July 2009, eventually producing a 5.4×10^7 m^3 dome (dense rock equivalent volume) (Diefenbach et al., 2013). More details of the eruption chronology can be found in Schaefer et al. (2012) and Bull and Buurman (2013.

3. Methods

3.1. UV remote sensing of SO_2

Airborne and satellite-based UV remote sensing can be used to retrieve the abundance of SO_2 within volcanic plumes using scattered UV radiation and principles of absorption spectroscopy (Stoiber et al., 1983). Variations of the Lambert–Beer Law (e.g. Platt and Stutz, 2008) are used to calculate the SO_2 abundance within an atmospheric column, referred to as the SO_2 column density. Satellite derived slant column densities (SCD) are converted to vertical column densities (VCDs) using an air mass factor (AMF; where VCD = SCD/AMF) calculated either geometrically or through a radiative transfer model (Yang et al., 2007). Airborne data acquired with the instrument pointing to zenith represent VCDs. Throughout this manuscript we refer to both measured and derived VCD values as column density (CD).

3.2. Airborne measurements using a Correlation Spectrometer

Since the 1990s COSPEC (Stoiber et al., 1983) has been the primary tool to measure SO_2 emissions from Alaskan volcanoes (Doukas, 1995; Doukas and Gerlach, 1995; Doukas and McGee, 2007). During the 2009 Redoubt eruption, 11 gas observation flights were conducted within 1.5 h of OMI overpasses. During each flight measurements of SO_2 CD were collected from a fixed-wing aircraft using an upward-facing Barringer COSPEC V by flying below-plume traverses, perpendicular to plume direction, and downwind from the volcanic source (Doukas and McGee, 2007). Airborne SO_2 CDs were integrated across plume width and multiplied by the wind speed (proxy for plume speed) to derive SO_2 emission rate. Wind speeds were estimated during each gas observation flight according to the wind circle method described by Doukas (2002). Measurements of SO_2 CD were collected at 1 Hz along with simultaneous GPS measurements of time, latitude, longitude, and altitude. Additionally, during most gas observation flights in situ measurements of SO_2 (and other gases) were collected according to the contour method (Gerlach et al., 1997; Doukas and McGee, 2007; Kelly et al., 2013). Because ambient SO_2 concentrations are near zero, these in situ SO_2 measurements along with GPS locations allowed plume width and altitude to be accurately constrained. More details of these methods can be found in Werner et al. (2013) and Kelly et al. (2013).

Airborne measurements are not collected during explosive eruptions due to: (1) the hazards associated with flying near a volcano during an explosive eruption (Werner et al., 2011), (2) the significant attenuation of UV light by volcanic ash, which can prevent SO_2 from being accurately measured (Williams-Jones et al., 2008), and (3) the low temporal resolution of gas flights prohibiting total explosive SO_2 emissions from being fully captured (Werner et al., 2011, 2013). Therefore our comparison between OMI and airborne measurements is restricted to effusive-phase activity.

Table 1
Explosive-phase eruption chronology for the 2009 Mount Redoubt eruption.

Date (UTC)	Time (UTC)	Activity	Event no. [1]	Plume height [6] (km)	Lahar[2]	Pyroclastic density current [2]	Tephra[7]	Acoustic group ‡,4	Gliding harmonic tremor [5]
15-Mar-09	21:05	Phreatic explosion [1]	0	4.6					
20-Mar-09	12:00	Onset of 66 hour seismic swarm (end at 6:34 on 23 March) [3]							
23-Mar-09		Satellite observation of lava dome growth prior to Event 1 [1]							
23-Mar-09	6:38	Magmatic Explosion [1]	1	5.5				1	
23-Mar-09	7:02	Magmatic Explosion [1]	2	13.4				2	
23-Mar-09	8:14	Magmatic Explosion [1]	3	14.6	X			2	
23-Mar-09	9:39	Magmatic Explosion [1]	4	13.1	X			2	
23-Mar-09	12:31	Magmatic Explosion [1]	5	18.3	X			2	
24-Mar-09	3:41	Magmatic Explosion [1] Possible lava dome growth between Events 6 and 7 [1]	6	18.3	X	X?	X	2	
26-Mar-09	16:34	Magmatic Explosion [1]	7	8.2	X				
26-Mar-09	17:24	Magmatic Explosion [1]	8	18.9	X	X		2	
27-Mar-09	0:00	Onset of an 8 hour seismic swarm (end at 8:28 on 27 March) [3]							
27-Mar-09	7:47	Magmatic Explosion [1]	9	12.5	X			1	X
27-Mar-09	8:29	Magmatic Explosion [1]	10	14.9	X			3	X
27-Mar-09	16:39	Magmatic Explosion [1]	11	15.6	X	X		3	X
28-Mar-09	1:41	Magmatic Explosion [1]	12	14.6	X		X	3	X
28-Mar-09	3:25	Magmatic Explosion [1]	13	15.2	X	X?	X	3	X
28-Mar-09	7:20	Magmatic Explosion [1]	14	14.6		X?		3	X
28-Mar-09	9:20	Magmatic Explosion [1]	15	14.6	X	X		3	X
28-Mar-09	21:40	Magmatic Explosion [1]	16	5.2	X			3	
28-Mar-09	23:29	Magmatic Explosion [1]	17	12.5	X			3	
29-Mar-09	3:23	Magmatic Explosion [1] Lava dome growth between events 18 and 19 [2]	18	14.6	X	X	X	3	
29-Mar-09	7:50	Onset of 1 hour seismic swarm [3]							
2-Apr-09	19:00	Onset of 44 hour seismic swarm (end at 13:58 on 4 April) [3]							
4-Apr-09	13:58	Magmatic Explosion [1] Lava dome growth following Event 19 [2]	19	15.2	X	X	X	4	

References: [1] Schaefer et al. (2012); [2] Bull and Buurman (2013); [3] Buurman et al. (2013); [4] Fee et al. (2013); [5] Hotovec et al. (2013); [6] Schneider and Hoblitt (2013); and [7] Wallace et al. (2013).
‡ Group 1: >16 min. duration, multiple pulses, low acoustic energies, no ultra long period (ULP) energy.
‡ Group 2: >10 min. duration, sustained infrasound, with no significant variation in amplitude, high acoustic energies, some ULP energy.
‡ Group 3: short duration, high acoustic energies, impulsive onsets, and peak frequencies of ~0.1 Hz.
‡ Group 4: emergent onset, two main pulses with second pulse having high amplitudes and significant ULP energy.

3.3. Overview of the Ozone Monitoring Instrument

OMI is a hyperspectral UV and visible satellite sensor aboard NASA's Aura spacecraft that measures atmospheric abundances of several trace gas species, including SO_2 (Carn et al., 2007). Aura is a polar orbiting satellite, and with a 2600 km swath width and 13×24 km pixel size at nadir, OMI attains full daily global coverage (Levelt et al., 2006). OMI has been collecting continuous atmospheric measurements since it became operational in September 2004 (Carn et al., 2007). OMI's temporal resolution, consisting of 1 pass per day at equatorial latitudes and up to 3 passes per day at high latitudes, provides the opportunity to obtain a remote snapshot of volcanic SO_2 emissions on any day when emissions are above OMI's detection limit and not obscured by meteorological clouds. For this study, operational OMI SO_2 data products (OMSO2; downloaded from:http://mirador.gsfc.nasa.gov/cgi-bin/mirador/collectionlist.pl?keyword=omso2) are analyzed using OMIplot software (Carn, 2011). OMSO2 data contain SO_2 measurements derived from the Band Residual Difference (BRD) (Krotkov et al., 2006) and Linear Fit (LF) algorithms (Yang et al., 2007), which retrieve SO_2 CD from measured radiances in up to 10 discrete UV bands between 310 and 360 nm. OMIplot software is used to produce images of SO_2 CD over a user-defined area, to calculate plume SO_2 mass by integrating the SO_2 CD values over the plume area, and to distinguish real SO_2 from noise through the use of SO_2 absorption spectrum peaks and troughs. The operational OMI SO_2 algorithms require an a priori assumption of SO_2 vertical distribution, characterized by the SO_2 layer center of mass altitude (CMA). For each OMI footprint, OMSO2 data products provide four values of total SO_2 CD corresponding to the following a priori CMAs: (1) ~0.9 km, for SO_2 in the Planetary Boundary Layer (*PBL*); (2) ~2.5 km, for SO_2 in the lower troposphere (*TRL*); (3) ~7.5 km, for SO_2 in the mid-troposphere (*TRM*); and (4) ~17.5 km, for SO_2 in the upper troposphere or lower stratosphere (*STL*) (http://so2.gsfc.nasa.gov/Documentation/OMSO2Readme_V111_0818.htm; (Yang et al., 2007). PBL SO_2 CDs are derived using the BRD algorithm, but SO_2 CDs for the other altitudes are retrieved using the LF algorithm. The user must select the most appropriate SO_2 product for the prevailing geophysical conditions.

Since mid-2008, OMI measurements have been affected by a dynamic radiance anomaly, known as the 'row anomaly' (http://www.knmi.nl/omi/research/product/rowanomaly-background.php), which is believed to be a result of partial blockage of the OMI nadir viewing port. For the period of measurements considered here, the row anomaly impacted rows 29 through 45 (Fig. 2) and these rows were thus excluded from analysis.

Validation of OMI SO_2 CD measurements has been attempted for both anthropogenic emissions in the PBL (Krotkov et al., 2006, 2008) and for volcanic SO_2 emissions in the troposphere and stratosphere (Spinei et al., 2010; Carn et al., 2011; Carn and Lopez, 2011). Good qualitative agreement for the low altitude anthropogenic emissions (Krotkov et al., 2008) and strong quantitative agreement between ground-based and OMI measurements for higher altitude (7–17 km) SO_2 CD measured under optimal viewing conditions (Spinei et al., 2010), were found, while the challenges of comparing ground and satellite based measurements of different temporal and spatial resolutions were highlighted by Carn and Lopez (2011). We report here the first detailed comparison between OMI SO_2 data and airborne SO_2 CD measurements for high latitude volcanic SO_2 emissions at lower tropospheric altitudes (~3–6 km). Additionally, we consider a common challenge for satellite measurements of volcanic activity, namely that the volcanic SO_2 emissions are not spatially homogeneous and often cover only a fraction of an OMI pixel. This investigation also includes the first effort to validate OMI-derived SO_2 emission rates to allow satellite measurements to be integrated into typical volcano observatory SO_2 emissions datasets.

3.4. Column density comparison methods

Our comparisons between the high spatial resolution airborne measurements of SO_2 CD and the lower spatial resolution OMI measurements use the following criteria: airborne SO_2 CD measurements must be collected less than 90 min before or after an OMI overpass and have sufficient areal extent to allow the fraction of the OMI pixel containing volcanic SO_2 to be clearly defined (referred to as the plume pixel fraction). The airborne SO_2 CD measurements and OMSO2 data in KMZ format are plotted together in *Google Earth Pro*. Plume limits are defined for each airborne traverse when airborne SO_2 CD values are greater than or equal to 1 Dobson Unit (DU; the approximate level of background noise), and are extrapolated to the vent location to define the plume limits. The area of the individual OMI pixels is determined by overlaying OMPIXCOR data products (Kurosu and Celarier, 2010), which show the areal extent of individual pixels including pixel overlap, on top of the OMSO2 KMZ files and aligning the pixel boundaries. *Google Earth Pro* is used to create polygons that outline the perimeter of the plume, the individual pixels, and plume pixel fraction; and then to calculate the fractional area of the plume within each pixel. Airborne SO_2 CD measurements are partitioned into individual OMI pixels, and the average airborne SO_2 CD for each traverse within a plume pixel fraction is calculated (Fig. 3). On days when multiple traverses transected a single OMI pixel at different down-wind distances, the average of the spatially different traverses collected most closely in time with the OMI overpass is used. To allow the airborne and OMI SO_2 CD values to be directly compared, we converted the airborne measurements from units of ppm*m to DU, the CD units used by OMI. Gerlach (2003) showed that COSPEC CD values are independent of temperature and pressure such that 1 ppm*m is equal to 2.663×10^{-6} kg/m^2 for a plume at any altitude. We used this along with the conversion from DU to kg/m^2 (1 DU $= 2.85 \times 10^{-5}$ kg/m^2) to derive a conversion factor of 1 ppm*m $= 0.0934$ DU. Once the average airborne SO_2 CD for each pixel was converted to DU we calculated a corrected airborne SO_2 CD value for the pixel, $C_{c,}$ (DU):

$$C_c = \left(C_a \times F_p\right) + \left(C_b \times F_b\right) \quad (1)$$

where C_a is the average airborne SO_2 CD measured within the pixel (DU), F_p is the fraction of the pixel containing plume (>1 DU SO_2), C_b is the average background SO_2 CD value for the pixel, and F_b is the fraction of the pixel containing background (<1 DU SO_2). Because ambient air typically contains 0 DU SO_2, Eq. (1) simplifies to:

$$C_c = \left(C_a \times F_p\right). \quad (2)$$

This equation attempts to correct for the spatial differences between the airborne and OMI datasets, allowing these different measurements to be directly compared (Fig. 3).

Accurate plume altitudes from Redoubt Volcano are constrained via airborne methods. The average plume altitude during the effusive phase of the eruption for days with supporting airborne measurements was 3.8 km above sea level (Werner et al., 2013). The comparison between OMI and corrected airborne CD was conducted for both OMI *TRL* and *PBL* SO_2 retrievals, where the operational *PBL* data products were corrected using a corrected air mass factor based on the total ozone, solar zenith angle, and satellite viewing angle for the specific conditions at Redoubt Volcano according to the method of Krotkov et al. (2008). Both retrievals were used to determine if one exhibited a better agreement with corrected airborne SO_2 CD values, considering that a plume at 3 km altitude above sea level over mountainous terrain may be better retrieved using the plume altitude above terrain level. Average terrain heights (a function of plume direction) below the plume are used to determine the most appropriate CMA on that

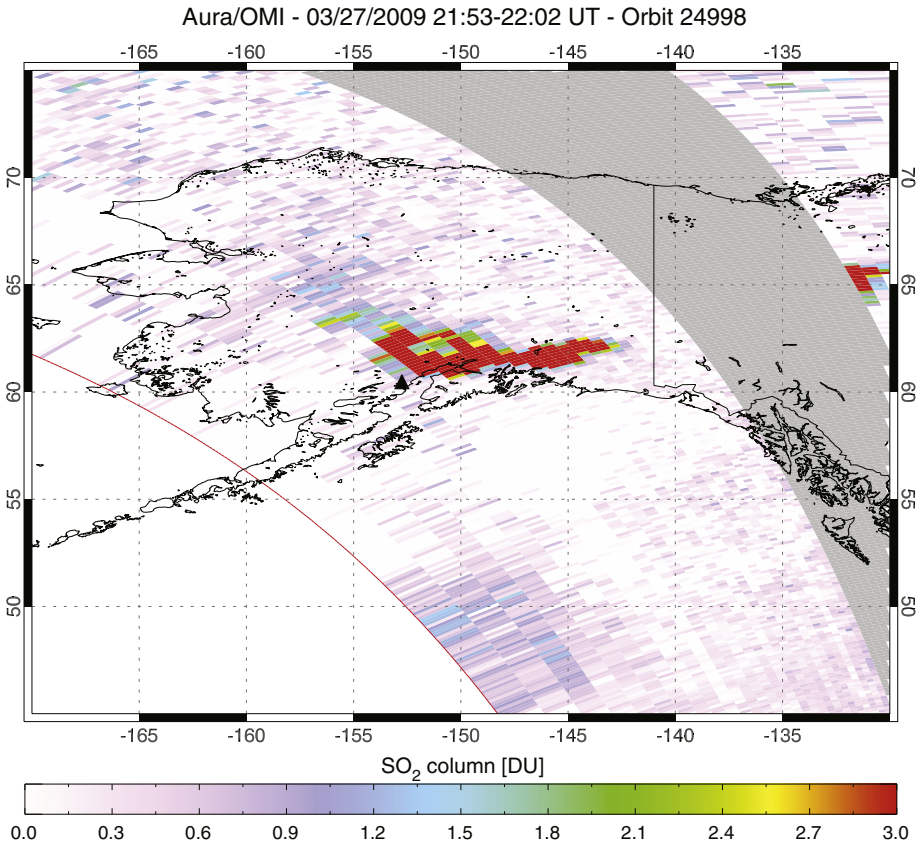

Fig. 2. Example OMI image from 27 March 2009 showing OMI SO_2 column density (CMA = 7.5 km) for Mount Redoubt's plume. The area shown is the analysis box. Redoubt Volcano is marked by a black triangle. The swath edge is outlined in red and the row anomaly pixels are shaded gray.

particular day, such that the *PBL* retrieval was used for plumes <2 km above terrain level and the *TRL* retrieval was used for plumes ≥2 km above terrain level. We refer to the most appropriate CMA as the *Selected* altitude. The comparison between OMI *PBL*, *TRL*, and *Selected* altitude SO_2 CD values and corrected airborne SO_2 CD values was conducted for 16 pixels observed during the study period. This comparison was repeated for a subset of pixels collected under optimal viewing conditions. According to the OMI User's Guide (http://disc.sci.gsfc.nasa.gov/Aura/additional/documentation/README.OMI_DUG.pdf) optimal conditions for OMI PBL SO_2 retrievals include: cloud fractions <0.2, solar zenith angle <50°, and near nadir satellite viewing angles (<45° from nadir). Considering these factors, a subset of 8 pixels collected under optimal conditions was evaluated, which we refer to as the optimal dataset. The results of the comparison between OMI and corrected airborne SO_2 CD values were evaluated through consideration of the percent difference, where we assume that corrected airborne SO_2 CD values are accurate and represent the true SO_2 CD in Mount Redoubt's plume at the time of the OMI overpass. This assumption is a simplification, as uncertainties in airborne CDs are estimated to be ±10% for cloud-free conditions, and spatial (downwind) and temporal variations in Mount Redoubt's SO_2 emission rates of 10% were observed on the scale of OMI pixels (Werner et al., 2013). However, we believe this assumption is justified as both the airborne SO_2 CD error and the observed variability in SO_2 emissions are quite low. We consider the advantage of utilizing multiple traverses in our analysis in order to provide more complete spatial coverage of OMI pixels to outweigh the negative effect of introducing minor variability in airborne measured emission rates by considering traverses collected within 90 min of an OMI overpass. The *TRL*, *PBL* and *Selected* SO_2 CD values were plotted against the corrected airborne SO_2 CD values to constrain the linear relationship and coefficient of determination (R^2) for each analysis. A linear relationship is expected between OMI and corrected airborne SO_2 CD values, as both methods measure the SO_2 CD of Mount Redoubt's plume, with the primary difference between the measurements being the spatial resolution.

3.5. OMI measurements of SO_2 mass

Measurements of SO_2 mass detected by OMI in Mount Redoubt's plume were calculated using a multistep process. First, OMI data for a 30°×40° box with coverage of Redoubt Volcano and the surrounding area (45° to 75° North latitude×170 to 130° West longitude) referred to as the analysis box (Fig. 2) were acquired. This box was selected to provide coverage of mainland Alaska and to include plumes up to ~1 day old for plume speeds of up to 14.5 m/s (the maximum wind speed observed from airborne methods) (Werner et al., 2013). The image was produced in footprint mode, which reflects the true shape and orientation of the OMI pixels. If elevated SO_2 emissions from Redoubt Volcano were detected in the OMI image, pixel SO_2 CD values within the apparent plume were verified using OMI ozone algorithm (OMTO3) residuals at four peaks and troughs within the SO_2 absorption spectrum, referred to as SO_2 index values (see Krotkov et al., 2006). If the SO_2 index values were consistent with SO_2 absorption, the plume was assumed to be real and the plume SO_2 mass and area within the analysis box were calculated. The mass of apparent SO_2 representing background conditions within a similar area was also calculated and subtracted from the plume SO_2 mass to correct for background noise. In the case that the entire SO_2 plume could not be contained within a single box (due to separate gas puffs or row anomaly pixels truncating the plume), then several boxes were analyzed and the resultant masses summed. If multiple OMI orbits contained coverage of Mount Redoubt's plume, the procedure was repeated for each orbit.

OMI typically provides three overpasses per day with coverage of Redoubt Volcano, though in this case often only one image per day had good coverage of the entire plume. The most representative mass calculated for each day's OMI images, including the best coverage of the plume and/or near-nadir viewing conditions, was selected to be the reported daily SO_2 mass (Table 2).

OMI images are "snapshots" of SO_2 emitted and require wind velocities and SO_2 loss rates to be accurately known to constrain the time period of SO_2 emission within the image. We assume that the total SO_2 mass does not change significantly over time scales of 1–3 h, the time period encompassing OMI's ~3 overpasses of Redoubt Volcano; and that the SO_2 present within the analysis box represents only SO_2 emitted by Redoubt Volcano over the preceding 24 h.

3.6. Plume speed and daily SO_2 emission rate calculation methods

We developed three simple algorithms to convert the OMI measured SO_2 masses (kg) into SO_2 emission rates (tons per day [t/d]) to facilitate comparison between the OMI and airborne data and allow direct integration of these datasets. OMI emission rate calculations require estimates of plume altitude and plume speed. On days when gas observation flights were conducted, plume altitude and speed were determined using the previously described airborne techniques (Section 3.2). On other days, local radiosonde data were used along with thermal infrared satellite data to estimate plume top altitudes (Webley et al., 2013), and wind speeds were estimated using the READY system and the HYSPLIT trajectory model with Global Data Assimilation System (GDAS) meteorological data (http://ready.arl.noaa.gov/index.php). Model outputs for the location of Redoubt Volcano, the closest time to the OMI overpass or airborne survey (within 1.5 h), and the observed plume altitude were used to determine the appropriate wind speed and direction. Fair agreement ($R^2 = 0.5$) between airborne and modeled wind speeds was observed with an average difference of ± 2 m/s (or 20%) and a maximum difference of ± 5 m/s (or 110%) suggesting that modeled wind data are an adequate alternative data source when airborne measurements are not possible. Once the plume speed had been estimated, it was used with the following methods to estimate daily SO_2 emission rate (t/d).

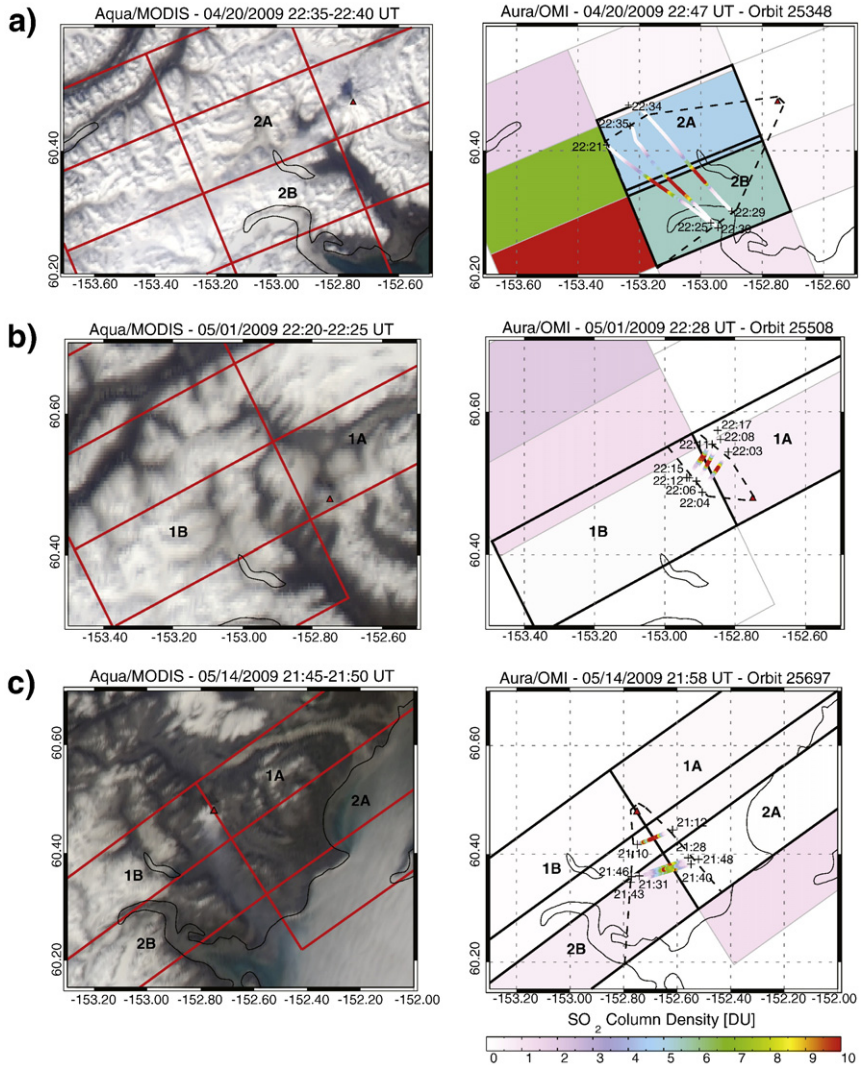

Fig. 3. Pixel column density comparison with airborne measurements for 16 pixels collected on 20 April (a), 1 May (b), 14 May (c), 26 May (d), 3 June (e), and 7 June (f). The left side of this figure shows Aqua MODIS visible imagery acquired within 15 min of the OMI overpass, with OMI tiled pixel areas outlined in red. Mount Redoubt's plume is visible in MODIS images on 20 April, 14 and 26 May, and 7 June. Surface reflectivity conditions for the analyzed days can be seen. The right side of this figure depicts the OMI measured SO_2 CD for tiled pixel areas with warmer colors representing higher CD values. Accurate pixel areas, including pixel overlap, for the analyzed pixels are outlined in black. Airborne SO_2 CD from the traverses used in the pixel analysis are plotted on top of the OMSO2 data using the same color bar scale, with traverse start and end times labeled. Plume limits, based on airborne CD measurements of SO_2 greater than or equal to 1 DU, are outlined in dashed black. Assigned pixel labels used in the analysis are shown and Redoubt Volcano is marked with a red triangle.

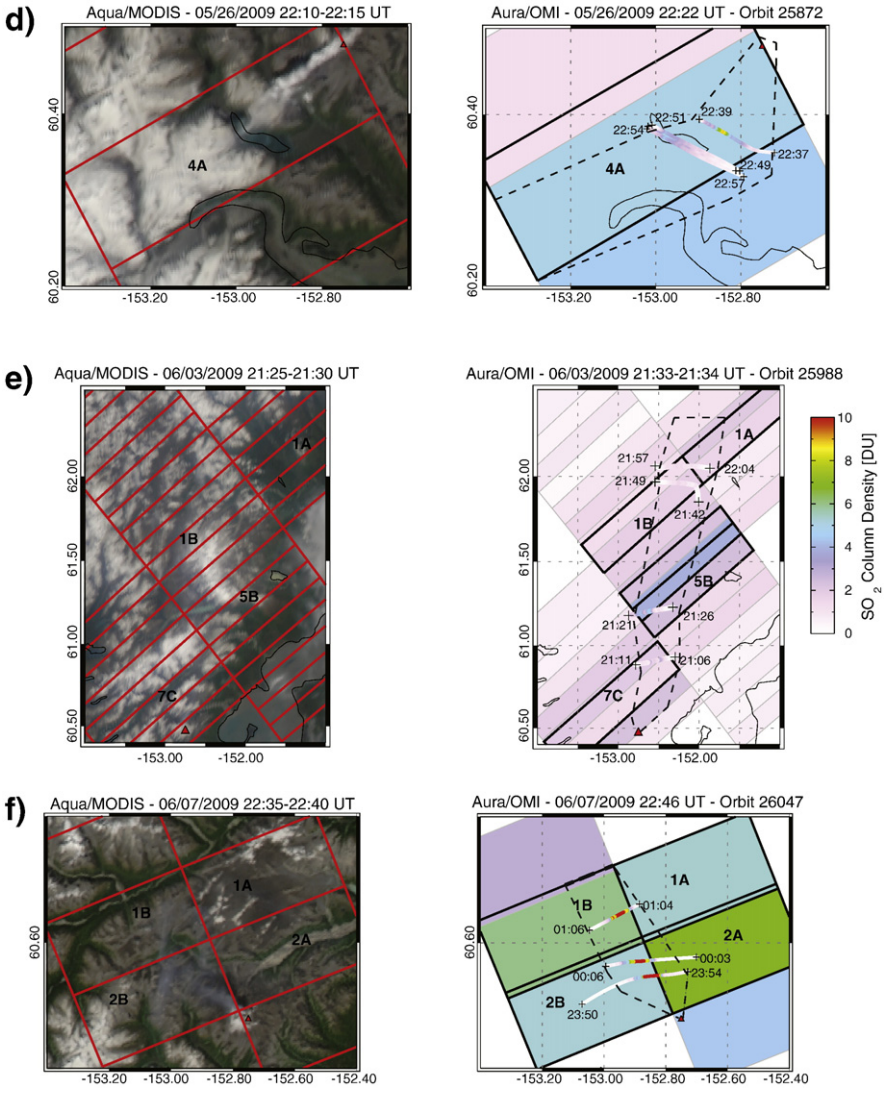

Fig. 3 (*continued*).

In *Method 1*, the SO_2 mass for each image (M), is multiplied by the wind speed (V), divided by the length of the plume in the direction of transport (L), and converted to t/d (Fig. 4a).

In *Method 2* (Fig. 4b), the wind speed (V) was used to calculate the distance the plume could have traveled in a period of 24 h (L_{24}). Next, the SO_2 mass was calculated for the 24 hour plume, providing an emission rate result in units of t/d. This method was only applied when L_{24} was contained within the analysis box, and the plume extended at least as far as L_{24}.

Method 3 uses the same principles as the airborne method to calculate SO_2 emission rates. Specifically, for plumes oriented parallel and/or perpendicular to a pixel boundary, the SO_2 CD within the pixel(s) was multiplied by plume width to calculate a plume SO_2 cross-sectional area in units of DU*m, which was then converted to kg/m ($1\ DU = 2.85 \times 10^{-5}\ kg/m^2$). This value was then multiplied by plume speed (m/s) to yield emission rate in kg/s, which was then converted to t/d.

The OMI-derived emission rates calculated using the three methods were compared to airborne SO_2 emission rates measured on 11 days during the eruption with near-coincident (within 1.5 h) OMI overpasses. Comparisons were not conducted on days with explosive eruptions as significant pulses of SO_2 were emitted during these explosions that were captured in OMI imagery but were not captured by airborne measurements.

4. Observations and results

4.1. Summary of observations

The study period for comparison of OMI and airborne SO_2 emission measurements was from 23 March 2009 through 12 June 2009 (Table 2). While SO_2 emissions from Redoubt Volcano continued past this date, the eruption of Sarychev Peak, Kurile Islands, Russia from 11 to 20 June 2009 (Rybin et al., 2011), produced large SO_2 clouds that traveled across the North Pacific preventing SO_2 from Redoubt Volcano from being accurately distinguished from that of Sarychev Peak. During our study period OMI detected SO_2 from Redoubt Volcano on 67 days, OMI data were not available on three days, and no SO_2 from Redoubt Volcano was detected by OMI on 12 days. Airborne SO_2 measurements were collected on 14 days during the study period (Werner et al., 2013). Airborne measurements on

Table 2
Data table of daily OMI measured SO_2 masses and derived emission rates (*Method 1*).

Date	Time	OMI orbit	Plume altitude [1,*]	OMI altitude algorithm used	Wind speed	OMI SO_2 mass	OMI M1 SO_2 emission rate	Airborne SO_2 emission rate*	Cumulative SO_2 mass	Cumulative SO_2 emission rate
	(UTC)		(km)		(m/s)	(kt)	(t/d)	(t/d)	(kt)	(kt)
3/14/2009	22:23	24809				0	0		0	0.0
3/15/2009	21:31	24823				0	0		0.0	0.0
3/16/2009	22:14	24838				0	0		0.0	0.0
3/17/2009	21:20	24852				0	0		0.0	0.0
3/18/2009	22:02	24867				0	0		0.0	0.0
3/19/2009	22:45	24882				0	0		0.0	0.0
3/20/2009	21:50	24896				0	0		0.0	0.0
3/21/2009	22:33	24911	NA	TRL	3.7	0.3	400		0.3	0.4
3/22/2009	21:38	24925				0	0		0.3	0.4
3/23/2009	20:40	24940	11	STL	13.07	54.4	71,400		54.7	71.8
3/24/2009	21:22	24954	10	STL	19.7	60.1	84,100		114.9	155.9
3/25/2009	No detectable plume					0	0		114.9	155.9
3/26/2009	21:10	24983	4*	TRL	5.4*	13.6	27,500	3590	128.4	183.4
3/27/2009	23:31	24999	9	STL	8.67	20.2	18,800		148.7	202.2
3/28/2009	20:58	25012	8	STL	31.1	38.5	75,000		187.2	277.2
3/29/2009	21:41	25027	10	STL	12.55	0.2	1200		187.3	278.4
3/30/2009	0:02	25043	7	STL	5.7	3.2	2900		190.5	281.3
3/31/2009	21:28	25056	6	STL	17.83	1.5	3000		192.0	284.3
4/1/2009	22:11	25071	7	STL	29.23	4.9	17,700		196.9	302.0
4/2/2009	No detectable plume					0	0		196.9	302.0
4/3/2009	21:59	25100	7.5	STL	14.13	3.8	6400		200.7	308.4
4/4/2009	21:04	25114	3.8	TRL	9.17	24.2	26,900	16,650	225.0	335.3
4/5/2009	No data		4.3					11,350	225.0	335.3
4/6/2009	22:30	25144	4	TRL	3.35	4.1	3600		229.0	338.9
4/7/2009	21:34	25158	7	STL	2.03	8.2	1900		237.3	340.8
4/8/2009	22:17	25173	7	STL	9.7	11.4	9800		248.6	350.6
4/9/2009	21:22		7	STL	15.4	12.3	10,400		261.0	361.0
4/10/2009	20:29	25201	8	STL	9.35	9.8	6000		270.8	367.0
4/11/2009	22:48	25217	11	STL	5.1	13.7	5500		284.5	372.5
4/12/2009	21:53	25213	8	STL	8.27	24.6	12,600		309.1	385.1
4/13/2009	20:58	25245	6	STL	28.1	7.5	10,800		316.6	395.9
4/14/2009	21:41	25260		STL	12.43	5.2	5800		321.8	401.7
4/15/2009	22:23	25289		STL	7.78	6.6	4100		328.3	405.8
4/16/2009	23:07	25290	4.1*	TRL	2.6*	8.0	2200	1950	336.3	408.0
4/17/2009	23:50	25305	9	STL	2.38	2.5	900		338.8	408.9
4/18/2009	0:33	25320	6	STL	12.85	10.9	6600		349.7	415.5
4/19/2009	21:59	25333	6	STL	9.2	10.6	6000		360.4	421.5
4/20/2009	22:42	25348	5.0*	TRL†	5.3*	14.0	8300	12,730	374.4	429.8
4/21/2009	21:47	25362		STL	18.9	1.8	5800		376.2	435.6
4/22/2009	22:30	25377		STL	18.23	3.8	4000		380.0	439.6
4/23/2009	Poor data coverage					0			380.0	439.6
4/24/2009	0:00	25407	6	STL	28.1	1.8	10,300		381.8	449.9
4/25/2009	21:22	25420		TRL	18	1.7	2600		383.5	452.5
4/26/2009	22:04	25435		TRL	14	2.8	6200		386.3	458.7
4/27/2009	21:10	25449		TRL	24.6	3.8	10,700		390.1	469.4
4/28/2009	21:53	25464	3.4*	TRL	10.7*	6.6	9620	13,280	396.7	479.0
4/29/2009	22:36	25479		TRL	9.4	2.3	3600		399.1	482.6
4/30/2009	21:40	25493		TRL	6.18	4.6	2000		403.7	484.6
5/1/2009	22:23	25508	3.5*	TRL	14.5*	4.8	5900	8370	408.5	490.5
5/2/2009	23:07	25523		TRL	5.5	6.6	3700		415.0	494.2
5/3/2009	22:11	25551		TRL	2.4	7.0	2500		422.0	496.7
5/4/2009	22:54	25552	3.5*	TRL	7.0*	13.1	7300	14,280	435.1	504.0
5/5/2009	21:59	25566		TRL	6.53	6.0	5800		441.1	509.8
5/6/2009	21:04	25580		TRL	8.45	13.2	8400		454.3	518.2
5/7/2009	No data					0			454.3	518.2
5/8/2009	22:29	25610	3.7*	TRL	7.6*	5.8	6600	6560	460.1	524.8
5/9/2009	21:34	25624	3	TRL	17.7	0.6	3200		460.7	528.0
5/10/2009	22:17	25639		TRL	12	3.8	2500		464.4	530.5
5/11/2009	Poor data coverage					0	0		464.4	530.5
5/12/2009	22:05	25668		TRL	5.33	1.6	600		466.0	531.1
5/13/2009	22:48	25683		TRL	5.9	3.5	1500		469.5	532.6
5/14/2009	21:52	25697	3.4*	TRL	7.6*	6.4	7600	8920	475.9	540.2
5/15/2009	22:36	25712		TRL	5.98	4.0	1800		479.9	542.0
5/16/2009	23:19	25727		TRL	5.68	1.4	600		481.3	542.6
5/17/2009	0:02	25742		TRL	7.95	1.7	4200		483.0	546.8
5/18/2009	No detectable plume					0	0		483.0	546.8
5/19/2009	22:11	25770		TRL	14.08	8.3	11,500		491.3	558.3
5/20/2009	22:54	25785		TRL	9.73	8.8	6400		500.1	564.7

(continued on next page)

Table 2 (*continued*)

Date	Time (UTC)	OMI orbit	Plume altitude [1,*] (km)	OMI altitude algorithm used	Wind speed (m/s)	OMI SO_2 mass (kt)	OMI M1 SO_2 emission rate (t/d)	Airborne SO_2 emission rate* (t/d)	Cumulative SO_2 mass (kt)	Cumulative SO_2 emission rate (kt)
5/21/2009	No detectable plume					0	0		500.1	564.7
5/22/2009	No detectable plume					0	0		500.1	564.7
5/23/2009	No detectable plume					0	0		500.1	564.7
5/24/2009	22:29	25843		TRL	3.73	2.8	1400		502.9	566.1
5/25/2009	No detectable plume					0	0		502.9	566.1
5/26/2009	22:17	25872	3.5*	TRL	6.3*	5.4	3900	4310	508.3	570.0
5/27/2009	21:22	25886		TRL	3.47	4.4	2400		512.7	572.4
5/28/2009	22:04	25901		TRL	7.6	4.6	3700		517.2	576.1
5/29/2009	21:09	25915		TRL	12.18	2.4	8100		519.6	584.2
5/30/2009	21:52	25930		TRL	8.78	3.1	3400		522.7	587.6
5/31/2009	22:35	25945		TRL	12.6	0.5	1800		523.2	589.4
6/1/2009	No detectable plume					0	0		523.2	589.4
6/2/2009	22:23	25974		TRL	11.95	0.7	4000		523.9	593.4
6/3/2009	21:28	25988	3.4*	TRL	4.0*	0.8	1100	4220	524.7	594.5
6/4/2009	No detectable plume					0	0		524.7	594.5
6/5/2009	No detectable plume					0	0		524.7	594.5
6/6/2009	21:58	26032		TRL	19.13	3.4	10,800		528.2	605.3
6/7/2009	22:41	26047	3.8*	TRL	4.9*	1.8	3000	5600	530.0	608.3
6/8/2009	No data					0	0		530.0	608.3
6/9/2009	22:29	26076		TRL	1.23	2.6	700		532.6	609.0
6/10/2009	21:34	26090		TRL	1.67	2.0	500		534.6	609.5
6/11/2009	22:16	26105	3.8*	TRL	3.8*	4.5	3500	4220	539.1	613.0
6/12/2009	23:00	26120		TRL	3.57	2.9	1800		542.0	614.8

[1] Estimated from thermal infrared data and the temperature–altitude method from Webley et al. (2013), unless marked by '*'.
[*] Determined from airborne measurements from Werner et al., (2013).
[†] According to airborne measurements plume center is at 2.7 km, therefore the TRL algorithm was used in this analysis.

11 days were suitable for comparison with OMI derived emission rates and 6 days were suitable for comparison with OMI pixel CD.

4.2. Column density comparison results

The data used in the comparison between OMI measured and corrected airborne SO_2 CD values calculated using the *TRL*, *PBL*, and *Selected* plume altitude algorithms can be found in Table 3, with the results summarized in Supplementary Material, Table A.1, and shown in Fig. 5. In general, for the 3 km ASL plume typically observed at Redoubt Volcano, the operational *TRL* algorithm underestimated SO_2 while the corrected *PBL* algorithm overestimated SO_2 relative to the corrected airborne values (Fig. 5). The strongest linear correlation between the OMI and corrected airborne CD values for the 16 pixel analysis was observed for the *PBL* algorithm ($R^2 = 0.75$), followed by the *Selected* algorithm ($R^2 = 0.71$), and a weak correlation was observed for the *TRL* algorithm ($R^2 = 0.38$). The *TRL* algorithm had the smallest average percent difference and smallest standard deviation between OMI and corrected airborne SO_2 CD values for both datasets.

No improvement in linear correlation, average percent difference, or standard deviation was observed from using the optimal dataset, with the exception of a small decrease in average percent difference for the *TRL* algorithm. When the *PBL* and *TRL* algorithms were compared to the *Selected* algorithm, the *Selected* algorithm exhibited a stronger linear correlation than the *TRL* algorithm, and showed minor improvements when compared to the *PBL* algorithm with respect to average percent difference and standard deviation. This suggests that the *Selected* algorithm does not significantly improve results over the standard algorithms with respect to plume altitude above terrain level. Overall the *PBL* algorithm for all pixels had the strongest linear correlation with airborne measurements, while the *TRL* algorithm for all pixels had the smallest average percent difference and standard deviation.

The average airborne SO_2 CD values not corrected for differences in spatial resolution were also compared to the *TRL*, *PBL* and *Selected* altitude algorithm SO_2 CD values. No correlation was found between these measurements ($R^2 < 0.1$ in all cases), suggesting that for sub-pixel plumes, the spatial correction is critical for OMI data to be accurately compared with airborne measurements.

4.3. Daily SO_2 masses and emission rates

OMI detected SO_2 emissions from Redoubt Volcano almost daily during both the explosive and effusive phases of the eruption (Fig. 6; Table 2). On 21 March, two days prior to the explosive phase onset, weak SO_2 emissions (<0.5 kt) from Redoubt Volcano were detected by OMI. The explosive phase daily SO_2 masses (23 March through 4 April) ranged from 60.1 kt (on 24 March) to below detection limit and exhibited a correlation with volcanic activity that is described in detail in Section 5.7 (Table 4). From 5 April–12 June effusive phase daily SO_2 masses were quite variable and ranged from 24.6 kt (on 12 April) to below detection limit (on multiple days). The daily SO_2 masses from Redoubt Volcano exhibited an overall decreasing trend with time, with average daily OMI SO_2 masses for the explosive phase ($n = 13$), the effusive phase ($n = 69$), and the entire study period ($n = 82$) of 17.3 kt, 4.7 kt, and 6.7 kt, respectively.

Daily OMI-derived *Method 1* SO_2 emission rates ranged from 84,100 t/d (on 24 March) to below detection limit (on multiple days), and followed a similar trend to the daily SO_2 masses (Fig. 6). The average *Method 1* emission rates for the explosive phase ($n = 13$), the effusive phase ($n = 69$), and the entire study period ($n = 82$) was 25,800 t/d,

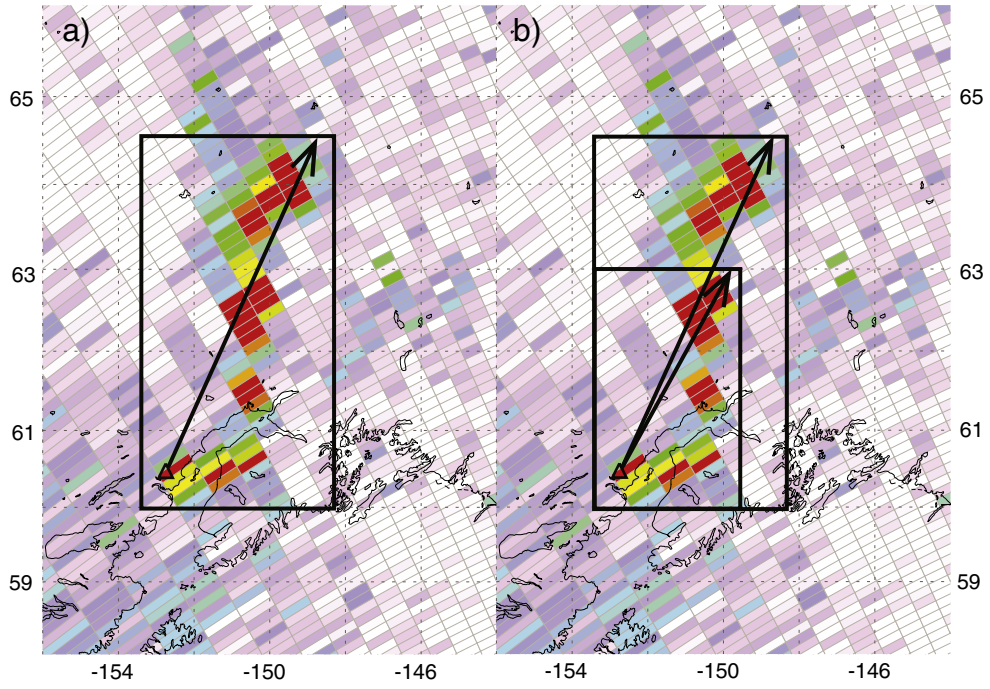

Fig. 4. OMI image from 6 June 2009 showing an SO_2 plume from Redoubt Volcano and two methods used to estimate SO_2 emission rate from OMI SO_2 mass. In *Method 1* (a), the mass, *M*, of the visible SO_2 plume is multiplied by the modeled plume speed, *V*, and divided by the plume length, *L* (black arrow), to obtain emission rate. In *Method 2* (b), the modeled plume speed, *V*, is used to calculate the distance the plume could travel in a period of 24 h, L_{24} (shorter, black arrow). The mass of the plume is calculated to L_{24} to provide a daily SO_2 emission rate.

4200 t/d, and 7800 t/d, respectively. The resultant emission rates calculated using these three methods were compared to airborne emission rates when available.

4.4. Emission rate calculation method comparison

Airborne SO_2 measurements collected on 11 days had near-coincident OMI images of passive degassing from Redoubt Volcano to allow SO_2 emission rates to be calculated using *Method 1*. Six days had both a near-coincident OMI overpass and a plume at least 24 h old contained within the OMI analysis box such that emission rates could be calculated using *Method 2*. Four days had SO_2 plumes that traveled parallel or perpendicular to the OMI pixel orientation, such that OMI emission rates could be calculated using *Method 3*. The results of the comparison are shown in Fig. 7 and summarized in Supplementary Material Table A.2. A strong linear correlation ($R^2 = 0.82$) between the OMI *Method 1* and airborne emission rates is observed, while weak and no correlations are observed for comparisons with OMI *Methods 2* and *3* ($R^2 = 0.34$ and 0.01), respectively. In almost all cases, OMI SO_2 emission rates are lower than respective airborne calculations.

4.5. Emission rate detection limit

OMI's emission rate detection limit for high latitude springtime conditions was estimated using observations of the maximum SO_2 emission rate determined from airborne measurements that corresponded with non-detection by OMI during the study period. Airborne SO_2 emission rates calculated for 15 and 20 March of 3850 and 940 t/d, respectively, corresponded with non-detection by OMI. In contrast, the remaining days within the sample period when both airborne and OMI emission rates were calculated found that emission rates as low as ~2000 t/d were detected by OMI. This may suggest that OMI's detection limit is >4000 t/d for early spring conditions and improves with increased UV radiation to <2000 t/d for mid to late spring conditions at Redoubt Volcano and other volcanoes at similar latitudes. It should be noted however, that the airborne measurements on 15 March were collected immediately prior to the phreatic explosion (Bull and Buurman, 2013) and as such these measurements may reflect a short-lived increase in SO_2 that may not be representative of that day's emissions on the spatial scale of an OMI pixel. Additional coincident low-magnitude (<4000 t/d) airborne and OMI SO_2 emission rate data are required to further constrain OMI's high latitude early springtime detection limit.

4.6. Cumulative SO_2 masses and emission rates for the study period

Daily OMI SO_2 masses and derived emission rates from Redoubt Volcano were summed from 19 March through 12 June to calculate the cumulative SO_2 mass emitted (Fig. 8). The total cumulative SO_2 mass emitted from Redoubt Volcano during this period as calculated from the daily masses (black diamonds) and *Method 1* emission rates (gray squares) was 542 kt and 615 kt, respectively. According to these values, approximately one half of the total SO_2 mass released during the study period was emitted during the explosive eruptive phase.

5. Discussion

5.1. Challenges and advantages of using OMI SO_2 data

Several aspects of OMI's temporal resolution, spatial resolution, and sensitivity to SO_2 were advantageous for this study. OMI's temporal resolution, typically 1 to 3 images per day with (full or partial) coverage of Mount Redoubt's plume, is significantly higher than what is possible through airborne methods. While OMI's spatial resolution is coarser than optimal for Mount Redoubt's average plume size (~6.2 km plume width at an ~11 km downwind distance according to Werner et al.,

Table 3
Summary of data used in the column density comparison.

Date	OMI orbit	Pixel label	Pixel center latitude	Pixel center longitude	TRL SO_2 CD (DU)	Air mass factor	Operation al PBL SO_2 CD (DU)	Corrected PBL SO_2 CD (DU)	Selected algorithm	Plume top (km ASL)	Plume thickness (km)	Plume pixel fraction	Average airborne SO_2 CD (DU)
4/20/2009	25348	2A	60.4327	−153.0690	4.92	0.30	39.74	47.13	PBL	5.0	3.1	0.71	26.6
4/20/2009	25348	2B	60.3191	−152.9760	5.44	0.30	42.80	51.01	PBL	5.0	3.1	0.73	56.9
5/1/2009	25508	1A	60.5762	−152.5870	0.66	0.38	2.74	2.59	PBL	3.5	1.7	0.07	46.9
5/1/2009	25508	1B	60.4295	−153.1430	0.25	0.37	2.09	2.02	PBL	3.5	1.7	0.06	34.7
5/14/2009	25697	1A	60.6374	−152.3050	0.33	0.35	1.40	1.45	TRL	3.4	1.3	0.03	56.3
5/14/2009	25697	2A	60.5340	−152.1720	0.10	0.35	1.83	1.90	TRL	3.4	1.3	0.08	23.8
5/14/2009	25697	1B	60.2998	−153.2440	0.16	0.34	0.33	0.35	TRL	3.4	1.3	0.03	78.2
5/14/2009	25697	2B	60.1970	−153.1100	0.82	0.34	2.97	3.13	TRL	3.4	1.3	0.16	41.5
5/26/2009	25872	4A	60.3651	−153.0360	5.02	0.37	20.04	19.73	TRL	4.0	1.9	0.52	23.8
6/3/2009	25988	1A	62.2600	−151.5250	1.63	0.34	4.33	4.56	PBL	3.4	1.4	0.30	7.3
6/3/2009	25988	1B	61.7780	−152.7010	1.86	0.33	6.91	7.50	PBL	3.4	1.4	0.36	9.9
6/3/2009	25988	5B	61.3920	−152.0740	2.41	0.33	7.17	7.89	PBL	3.4	1.4	0.41	23.4
6/3/2009	25988	7 C	60.6368	−153.0800	1.39	0.32	3.96	4.51	PBL	3.4	1.4	0.27	13.2
6/7/2009	26047	2A	60.5909	−152.6110	6.76	0.40	24.78	22.37	PBL	4.9	1.1	0.16	14.35
6/7/2009	26047	1B	60.6176	−153.1410	6.00	0.40	23.30	21.03	PBL	4.9	1.1	0.31	54
6/7/2009	26047	2B	60.5040	−153.0480	5.27	0.40	23.18	21.04	PBL	4.9	1.1	0.21	62.75

[a] Optimal pixels contained cloud fractions <0.2, solar zenith angle <50°, and satellite viewing angle less than 45°.

2013), it is the highest spatial resolution of current UV satellite sensors. Many infrared sensors (e.g. AIRS, MODIS) have higher temporal and/or spatial resolutions than OMI (Thomas and Watson, 2009), but are less sensitive to SO_2, especially for low altitude plumes (Carn et al., 2005; Prata and Bernardo, 2007; Thomas et al., 2009) such as often observed at Redoubt Volcano. OMI's sensitivity to SO_2 combined with its temporal and spatial resolution allowed detection of Mount Redoubt's plume on approximately 80% of the analyzed days, many of which were ~3 km or less in altitude. Additionally, OMI detected SO_2 throughout the explosive phase when airborne measurements were not possible. This large percentage of detected plumes would not have been possible with other available sensors or through airborne methods alone, making OMI the ideal tool for this study as it provided nearly daily measurements of Mount Redoubt's SO_2 emissions.

There are two main challenges in using OMI data for this study that are unique to OMI and/or UV sensors in general. First OMI's row anomaly often truncated plumes within the OMI image, frequently limiting the number of usable daily images of Mount Redoubt's plume to one. Secondly, as a consequence of Redoubt Volcano's high latitude location and resultant high solar zenith angles in winter months, significant UV attenuation contributed to relatively low signal to noise in early spring images (Bluth et al., 1993). The main challenges of this study, however, are inherent to the fundamental differences in data collection methods between airborne and satellite measurements. We will discuss these challenges in more detail with respect to CD, mass, and derived emission rates in the following sections.

5.2. Uncertainties in airborne SO_2 measurements

Throughout this study we compare OMI satellite to airborne COSPEC SO_2 measurements. Airborne measurements by COSPEC have limitations such that they may not represent true daily SO_2 emissions, and thus these uncertainties should be considered in the context of the comparison with OMI measurements. The primary factors that contribute to uncertainty in COSPEC airborne SO_2 emission rate calculations include uncertainty in: (1) calibration cell concentration, (2) plume speed, and (3) retrieved SO_2 CD due to molecular scattering and dilution (Stoiber et al., 1983). While the uncertainty in calibration cell concentration (~5% (Stoiber et al., 1983; Werner et al., 2013)) and plume speed (~5% (Doukas, 2002)) are fairly minor components, uncertainties in SO_2 CD due to molecular scattering and dilution could be up to a an order of magnitude (Kern et al., 2010). Because airborne measurements were made directly under the plume, scattering and dilution error are minimized (Kern et al., 2010; Werner et al., 2013). The overall uncertainty in airborne SO_2 CD and calculated emission rates is therefore estimated to be ±10% and ±20%, respectively, for cloud-free conditions (Werner et al., 2013).

5.3. Evaluation of column density analysis

There are several challenges in comparing OMI and airborne CDs that can contribute to deviations from a linear relationship. First, the temporal and spatial differences between OMI and airborne methods along with the variability of Mount Redoubt's emissions make direct comparison between these measurements challenging. OMI acquires an image of Mount Redoubt's plume in less than one minute, while a representative number of airborne plume traverses (5–7) may take over 1 h to collect. Changes in SO_2 emissions during the period of airborne measurements can contribute to discrepancies between the two datasets. Additionally, because OMI acquires an image of the entire plume, while the airborne measurements only sample a localized cross-section of the plume, it is possible that spatial variability in SO_2 emissions may be more fully captured by OMI. Four to seven airborne SO_2 CD traverses were conducted on the six days evaluated. On five out of six of the days, traverses were collected within 85 minute time periods at distances up to 12 km apart. The average variability in the integrated plume SO_2 area (i.e. SO_2 CD integrated over the plume width) with respect to the mean was ±8%, while the maximum variability was ±23%. This suggests that the down-wind variability in SO_2 emissions on pixel-sized scales will likely be between ±8 and ±23%.

A second concern related to the spatial variability between the OMI and airborne datasets is due to the relatively small plume size compared to the OMI pixel size. Of the 16 pixels analyzed, the highest plume pixel fraction was 0.73, and the average plume pixel fraction was 0.27. The calculation designed to account for the spatial differences between OMI pixels and airborne measurements (Section 3.4) depends on OMI SO_2 CD, in addition to accuracy of the traverse plume limit locations, the interpolated plume limits, and area of the pixels and plume fractions. We compare OMI pixel areas from the OMPIXCOR data product (Kurosu and Celarier, 2010) to pixel areas determined in *Google Earth Pro* and find a maximum percent difference between these datasets of 4, with an average percent difference

Corrected airborne SO_2 CD (DU)	Percent difference between OMI and airborne SO_2 CD TRL	Percent difference between OMI and airborne SO_2 CD PBL	Percent difference between OMI and airborne SO_2 CD Selected	Total column ozone (DU)	Satellite viewing angle (°)	Solar zenith angle (°)	Aerosol index	Cloud fraction	Minutes elapsed between OMI and airborne Measurements	Optimal conditions [a]
18.80	−73.9	150.6	151	494.0	18	49	−1.74	0.00	−44 to −3	Yes
41.67	−87.0	22.4	22	497.6	18	49	−1.91	0.00	−44 to −3	Yes
3.23	−79.5	−19.8	−20	338.5	34	45	0.68	0.00	−29 to −6	Yes
1.95	−87.3	3.5	4	349.3	36	45	1.26	0.00	−29 to −6	Yes
1.69	−80.4	−13.7	−80.4	355.7	52	42	−0.26	0.00	−51 to −6	No
1.93	−94.8	−1.6	−94.8	355.8	52	42	−0.26	0.00	−51 to −6	No
2.38	−93.3	−85.4	−93.3	353.4	55	42	2.70	0.00	−51 to −6	No
6.55	−87.5	−52.2	−87.5	353.9	55	41	2.72	0.00	−51 to −6	No
12.26	−59.1	60.8	−59.1	369.9	40	39	1.09	0.19	+20 to +40	Yes
2.17	−25.0	109.7	110	342.2	57	40	−0.27	0.04	−22 to +78	No
3.53	−47.4	112.6	113	342.2	60	40	−1.03	0.18	−22 to +78	No
9.69	−75.1	−18.6	−19	349.7	60	39	−1.09	0.15	−22 to +78	No
3.50	−60.3	28.9	29	347.9	63	39	−1.30	0.21	−22 to +78	No
2.27	198.2	887.6	888	344.3	16	38	−1.05	0.00	+69 to +85	Yes
16.98	−64.7	23.9	24	342.3	18	38	−1.24	0.00	+69 to +85	Yes
13.32	−60.4	58.0	58	347.5	18	38	−0.40	0.00	+69 to +85	Yes

of 1.3. This suggests that our method for determining pixel area is relatively robust. Uncertainties in the plume pixel fraction areas will likely be larger as these values depend on several intermediate calculations.

Third, as shown by the CD comparison analysis, OMI CD values are strongly dependent on the selected plume CMA algorithm, indicating that accurate plume altitude and thickness constraints are critical to accurate OMI CD retrieval. Discrepancies between the actual plume CMA and the assumed CMA used in the *TRL* (2.5 km) and *PBL* (0.9 km) retrievals could contribute to error in retrieved CD.

Finally, spatial variations in and deviations from the assumed atmospheric conditions at Redoubt Volcano, specifically with respect to total ozone column, surface reflectivity, cloud cover, solar zenith angle, presence of ash and/or aerosols, etc. will contribute to uncertainties in OMI CDs. For conditions similar to those observed at Redoubt Volcano (unpolluted atmosphere with CDs less than 100 DU) the estimated uncertainty in CD for the LF and BRD algorithms is ±20% (Yang et al., 2007), and −7 to −23% (Krotkov et al., 2008), respectively. It should be noted that for pixels containing SO_2 plumes above highly reflective snow or clouds, SO_2 CD calculated using the *BRD* retrieval may be overestimated (Krotkov et al., 2008). Fig. 3 shows visible MODIS imagery of Redoubt's plume and surroundings (acquired within 15 min of the OMI overpass) with OMI pixels boundaries outlined in red, such that reflectivity can be evaluated. In particular high surface reflectivity observed on 20 April may be contributing to the anomalously high SO_2 CD values retrieved from the BRD retrieval on that day (Table 3).

A comparison between the percent difference between OMI (*TRL*) and airborne SO_2 CD values and other parameters including: total column ozone, satellite viewing angle, solar zenith angle, Aerosol Index, cloud fraction, plume altitude, and plume pixel fraction, was conducted for the 16 analyzed pixels (Table 3). No correlation was found between the percent difference and any of these parameters (maximum observed $R^2 = 0.1$), suggesting that no single parameter contributes significantly to the observed discrepancies. The pixel analysis associated with Pixel 2A on 7 June 2009 had the largest observed discrepancy with airborne measurements of ~198% (*TRL* retrieval). This pixel has the following characteristics: (1) a small plume pixel fraction (0.16), (2) a low average airborne CD (2.27 DU), (3) a relatively long time lag between OMI and airborne measurements (69 to 85 min), (4) a low surface reflectivity, and (5) the plume location was on the edge of the pixel (Fig. 3; Table 3). These observations suggest that the combined effects of several non-ideal factors can contribute to large disagreements between OMI and airborne CDs.

The above uncertainties in OMI and corrected airborne SO_2 CDs all contribute in part to the deviations in linearity between these datasets. Our findings suggest that the overall uncertainties in OMI SO_2 CD as determined through comparison with airborne measurements are on average −55% and +79% for the *TRL* and *PBL* retrieval's, respectively (see Supplementary Material, Table A.1 for more details).

5.4. Evaluation of daily SO_2 mass

We expect the error in the OMI SO_2 mass values to come from three primary sources: (1) error in the SO_2 CD, (2) error in the selected background noise level, and (3) error in the assumption that measured SO_2 is <1 day old. Errors in SO_2 CD were discussed previously and are not repeated here.

Variable background noise in the acquired OMI SO_2 images impacted the precision of the calculated daily SO_2 masses. Based on repeat processing of multiple OMI images in which different areas of background noise were subtracted from the measured plume SO_2 mass, we expect an uncertainty in precision for the reported SO_2 masses due to variability in background noise to be ~20%.

Another challenge in calculating daily SO_2 mass and emission rates (*Methods 1* and *2*) from satellite data is to include all the SO_2 emitted in the preceding 24 h. If we assume a consistent wind direction, wind speed, and a continuous SO_2 source, we can estimate plume age based on the wind speed and the length of the plume as measured by OMI. If we consider the OMI analysis box (45°–75°N, 130°–170°W) and a plume speed of 14.5 m/s (the maximum wind speed observed from Mount Redoubt 2009 airborne measurements (Werner et al., 2013)), a plume from Redoubt Volcano could reach the eastern extent of the analysis box (~1200 km) in ~1 day. For wind speeds greater than 14.5 m/s, OMI SO_2 mass will be underestimated, whereas for wind speeds less than 14.5 m/s, OMI SO_2 mass will be overestimated. Assuming that the ideal conditions mentioned above persisted throughout the sample period (a simplification), and using the wind speeds and plume lengths used for emission rate *Method 1* calculations, we find that our mass measurements may be overestimated on over half the days, with an average plume age of 1.2 days for the sample period. However, no correlation between SO_2 mass and plume age was observed, suggesting that this source of uncertainty may be minimal. An additional aspect to be considered is the chemical loss of SO_2 within volcanic plumes due to

homogenous or heterogeneous reactions, which can also cause OMI to underestimate daily SO_2 emissions (Pfeffer et al., 2006; Bluth and Carn, 2008; Rodriguez et al., 2008). Estimated SO_2 loss rates from the Mount Redoubt 1989–90 eruption were calculated to be $<2.8\times10^{-6}\ s^{-1}$ for tropospheric plumes, suggesting that SO_2 loss at Redoubt Volcano may be negligible over the course of a day (Hobbs et al., 1991; Casadevall et al., 1994; Oppenheimer et al., 1998). However, dispersion of SO_2 by advection and diffusion could also act to lower SO_2 CDs below OMI's detection limit during plume transport.

These various factors can contribute to uncertainties in the daily OMI SO_2 masses, however unlike OMI SO_2 CD and derived emission rates that can be validated using airborne measurements, there are no complementary data available to allow us to estimate the overall uncertainties in the daily SO_2 masses.

5.5. Evaluation of OMI-derived emission rates

Each of the emission rate calculation methods has advantages and disadvantages with respect to temporal resolution, processing time required, and measurement uncertainties. *Method 1* is the simplest method and can be applied to all days in which OMI SO_2 masses were calculated. This method produces the highest possible temporal resolution dataset; however it does not consider the age of the plume, so it is possible that *Method 1* may incorporate SO_2 from the previous day's emissions. *Method 2* does considers plume age in the emission rate calculation, but is only applied to days in which the 24 hour old plume extends to L_{24}, thus limiting the temporal resolution of this dataset. *Method 3* uses the same theory as the airborne emission rate calculation method and should theoretically agree most closely with airborne measurements. Additionally, because this method utilizes the plume SO_2 cross-sectional area near the source, factors such as plume dispersion, dilution, and SO_2 loss are minimized. However, *Method 3* is only applied when the volcanic plume is oriented parallel or perpendicular to an OMI pixel boundary, limiting the opportunities to use this method and resulting in poor temporal resolution. Analysis of *Methods 2* and *3* require more processing time than *Method 1*.

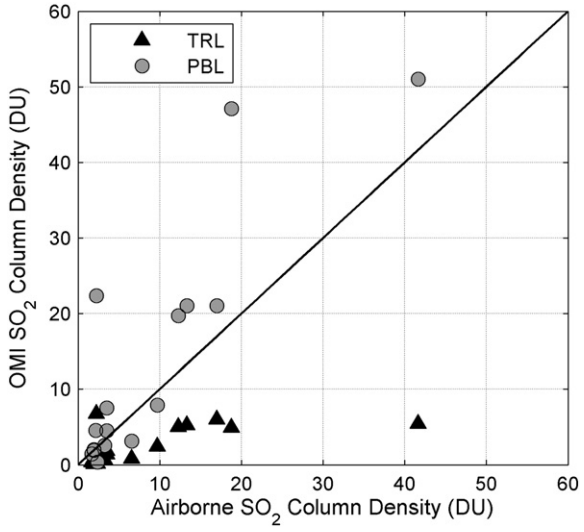

Fig. 5. Comparison between corrected airborne and OMI SO_2 CD for *TRL* (triangles) and *PBL* (gray circles) retrievals. The black line represents a 1:1 correlation. Uncertainties in airborne SO_2 CD are estimated to be ±10% (Werner et al., 2013). Uncertainties in retrieved OMI SO_2 CD for non-polluted conditions are estimated to be −7 to −23% (Krotkov et al., 2008) and ±20% (Yang et al., 2007) for the BRD and LF algorithms, respectively. Average differences between OMI *TRL*, *PBL*, and *Selected* SO_2 CDs and airborne SO_2 CDs are −55%, 79%, and 59%, respectively.

The uncertainties in the OMI-derived emission rates will include the uncertainties associated with SO_2 mass (*Methods 1* and *2*) and CD (*Method 3*) calculations described above (Sections 5.4 and 5.3, respectively), in addition to the uncertainties in plume speed and length. Of particular note is that the *Method 1* emission rates were calculated using the daily mass associated with the estimated plume top height. For example, a 3 km plume emission rate was estimated using the daily mass from the *TRL* CMA algorithm. The pixel analysis (Section 4.2) found that OMI SO_2 CD estimated from the *TRL* algorithm consistently underestimated SO_2 amounts; hence emission rates derived using *TRL* SO_2 data will also be biased low.

Because all three emission rate methods use plume speed in their calculations, the aforementioned plume speed uncertainties (Section 3.6) (average of ±2 m/s, max of ±5 m/s) will contribute to the uncertainties in all three emission rate methods. Uncertainties in plume length for *Methods 1* and *2*, are strongly dependent on the wind direction on the day preceding the image acquisition. For ideal conditions, including consistent wind direction, low image noise level, and well defined plume limits, we expect uncertainties in plume length to be ~15%. Often wind direction and speeds are variable, making it challenging to determine the appropriate plume length.

While there are clear sources of positive and negative error in the OMI-derived emission rates, the observations suggest that in most cases these values are lower than airborne measurements. Overall differences between OMI-derived and airborne emission rates are on average −28, −34, and −40%, for *Methods 1*, *2*, and *3*, respectively (see Supplementary Material, Table A.2 for more details). Good agreement between OMI *Method 1* and airborne SO_2 emission rates suggests that the former can be used as a reliable proxy for airborne measurements during passive degassing activity. The strong linear correlation between airborne and OMI *Method 1* data suggests that the equation of fit (Supplementary Material, Table A.2) could potentially be used to correct for OMI underestimation, allowing the OMI data to be better integrated with the airborne emissions dataset. Further testing is required to determine if this correction could be applied to other volcanoes observed by OMI under conditions similar to this study.

5.6. Discussion of cumulative SO_2 masses

Cumulative SO_2 masses were calculated from daily OMI measured masses and derived emission rates from 19 March through 12 June 2009 and determined to be ~542 and ~615 kt, respectively (Fig. 8). Approximately half of the OMI measured cumulative emissions for this study period were emitted during the explosive phase (225 kt from daily masses and 335 kt from daily emission rates), with the rest emitted during the pre-eruptive and effusive phases. The large fraction of cumulative SO_2 mass emitted during the explosive phase is significant because airborne methods are not capable of fully capturing these explosive SO_2 emissions (Section 3.2). This highlights OMI's utility as a volcano monitoring tool as it is able to quantify explosive SO_2 emissions and thus provide useful information that cannot be attained through airborne methods alone. It should be noted that the cumulative SO_2 masses estimated by OMI are lower than that estimated from airborne measurements (751.89 kt) for the same time period by approximately 30% and 20% for OMI mass and emission rate methods, respectively (Werner et al., 2013); however, the cumulative airborne SO_2 mass, calculated by linearly interpolating daily SO_2 mass values, assumes that SO_2 emissions are fairly consistent over time-scales of days to weeks and thus involves a certain degree of uncertainty.

The explosive and effusive phase cumulative OMI-derived SO_2 masses emitted during Mount Redoubt's 2009 eruption were similar to those estimated for the 1989–90 Mount Redoubt eruption using Total Ozone Mapping Spectrometer (TOMS) satellite SO_2 masses and airborne SO_2 emission rates (Casadevall et al., 1994; Schnetzler et al., 1994). Specifically, the cumulative SO_2 mass emitted during the

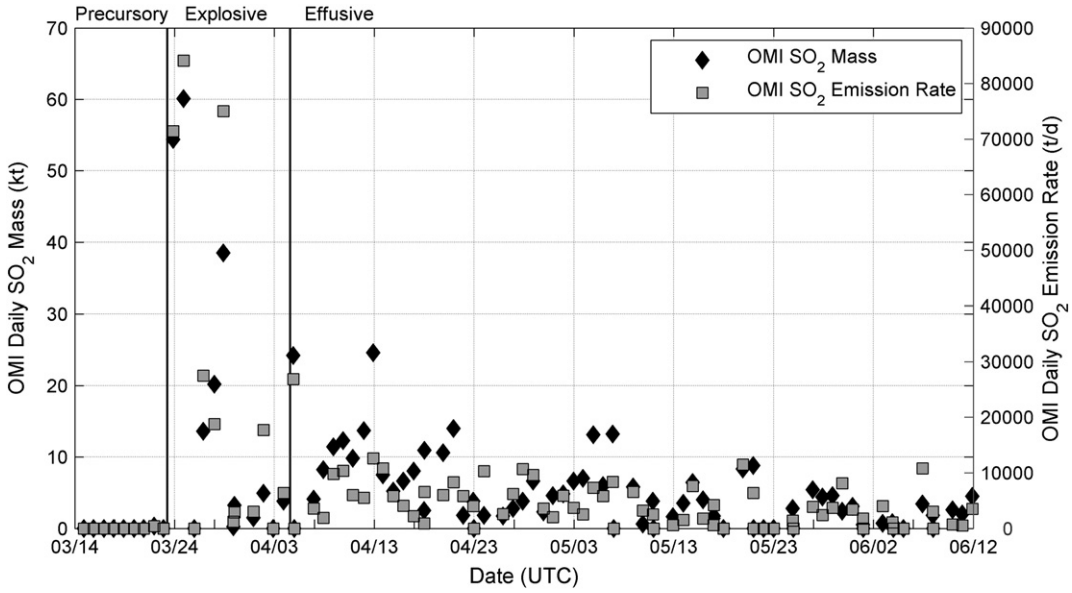

Fig. 6. OMI daily SO_2 mass (kt) (black diamonds) and OMI Method 1 calculated SO_2 emission rates (gray squares) from Redoubt Volcano. The black vertical lines represent the temporal breaks between precursory (left), explosive (center), and effusive (right) phases of the eruption.

explosive phase in 1989–90 was estimated to be ~175 kt ± 50 kt (Casadevall et al., 1994), which is similar to the SO_2 yield for the 2009 explosive phase reported here. The cumulative SO_2 masses estimated for the dome growth and destruction phase of the 1989–90 eruption (the phase most similar to the 2009 effusive phase) were estimated to range from 572 to 680 kt ± 90 kt (Casadevall et al., 1994). These values are approximately double those observed during the 2009 effusive phase; however the time period analyzed was 176 days in 1989–90, as opposed to the 69 days analyzed during the 2009 eruption.

5.7. Correlations between eruptive activity and OMI-derived SO_2 measurements

The relatively high temporal resolution of OMI daily SO_2 mass measurements allows these data to be compared with observations of volcanic activity and other geophysical datasets. In particular, high variability in the OMI SO_2 masses was observed during the explosive phase of Mount Redoubt's 2009 eruption that qualitatively agree with the timing of explosive events described by Bull and Buurman (2013). Additionally a strong correlation between cumulative daily SO_2 mass and relative acoustic energy ($r = 0.996$, according to the Spearman Rank Correlation Test) throughout the explosive phase of the eruption was observed and described in detail by Fee et al. (2013). This suggests that SO_2 mass measured following explosive activity may be used to evaluate relative eruption explosivity (Fee et al., 2010). Finally, a strong linear correlation ($R^2 = 0.97$) is exhibited between OMI SO_2 and tephra masses associated with the explosive events (Fig. 9) (Wallace et al., 2013). This suggests that comparable amounts of SO_2 and tephra were emitted during each day during the explosive phase, such that OMI SO_2 masses from explosive events are used as a proxy for relative eruption size, supporting the findings by Blake (2003). We group the daily SO_2 masses observed during the explosive phase into three categories: high (>10 kt), moderate (1 to 10 kt), and low (<1 kt) (Table 4), and in doing so the following correlations emerge: (1) high OMI SO_2 masses were observed on days corresponding with Events 1–6, 8–15, and 19 (Schaefer et al., 2012); (2) moderate SO_2 masses were observed on days in which no explosive eruptions occurred, but on which lava extrusion was suspected and/or observed by satellite imagery (Bull and Buurman, 2013); and (3) low SO_2 masses were observed on days in which little volcanic activity was observed (though dome growth is expected) (Table 4). An

Table 4
Daily OMI SO_2 masses and *Method 1* emission rates for Redoubt Volcano's explosive phase compared with explosive event timing.

Events	UTC date	Overpass time	Daily SO_2 mass (kt)	Daily M1 SO_2 emission rate (t/d)	Hours since last explosion	Qualitative SO_2 level[a]
1–5	3/23/2009	20:40	54.4	71,400	8:09	High
6	3/24/2009	21:22	60.1	84,100	17:41	High
	3/25/2009	23:44	0.0	0		Low
7–8	3/26/2009	21:10	13.6	27,500	3:46	High
9–11	3/27/2009	23:31	20.2	18,800	6:52	High
12–15	3/28/2009	20:58	38.5	75,000	11:38	High
16–18	3/29/2009	21:41	0.2	1200	18:18	Low
	3/30/2009	00:02	3.2	2900		Moderate
	3/31/2009	21:28	1.5	3000		Moderate
	4/1/2009	22:11	5.0	17,700		Moderate
	4/2/2009	21:16	0.0	0		Low
	4/3/2009	21:59	3.8	6400		Moderate
19	4/4/2009	21:04	24.2	26,900	7:06	High

[a] Qualitative levels: High ≥ 10 kt; 1 < Moderate < 10 kt; Low ≤ 1 kt SO_2.

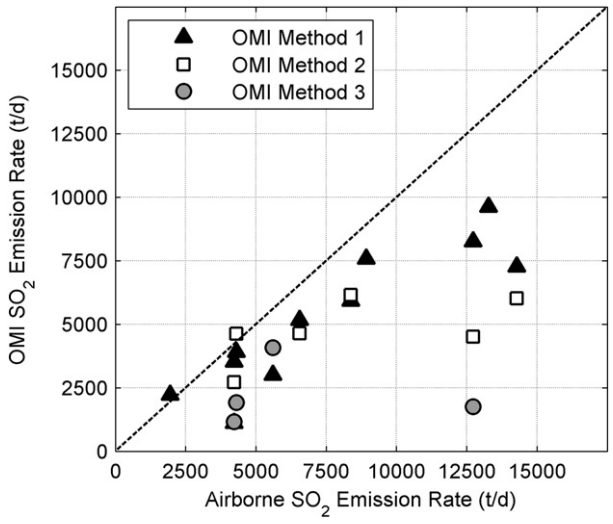

Fig. 7. Results of comparison between OMI-derived and airborne SO_2 emission rates. The dashed line represents a 1:1 correlation. Average differences between OMI-derived and airborne SO_2 emission rates for OMI *Methods 1*, *2*, and *3* are −28%, −34%, and −40%, respectively. OMI methods underestimate SO_2 emission rates relative to airborne measurements in almost all cases.

exception to (3) occurred on 29 March, when Events 16–18 occurred yet only 0.2 kt of SO_2 was detected.

Using the combined observations of SO_2 emission levels and eruptive activity we propose the following interpretations to describe Mount Redoubt's eruptive activity. First, high SO_2 masses observed were associated with explosive Events 1–5, 7–15, and 19, corresponding with the rapid eruption of a gas-rich magma. The moderate-level SO_2 emissions corresponded temporally with periods of dome growth (as observed from satellite imagery) and the absence of explosive eruptions (Table 4) (Bull and Buurman, 2013). We interpret these moderate-level SO_2 emissions to be due to slow degassing of a shallow or extruding magma. Low SO_2 emissions were observed on three days during the explosive phase, two of which had no explosive events (25 March and 2 April). One possible interpretation of the low SO_2 emissions observed on these dates is limited degassing through a viscous dome, and satellite imagery supports the presence of two domes between Events 6 and 7, and Events 18 and 19, respectively (Bull and Buurman, 2013). An alternate explanation is that due to poor OMI viewing conditions, the SO_2 emissions may have been below OMI's detection limit. The third day with observed low OMI SO_2 emissions occurred on 29 March when explosive Events 16, 17, and 18 occurred at least 19 h prior to the OMI overpass. We propose that the low SO_2 masses measured following these events may have been due to: (1) the long lag time between emission and OMI observations enabling the plume to become sufficiently dilute such that OMI only measured low SO_2 masses, and/or (2) these events having smaller eruption mass or lower volatile content and thus less explosive than the other events, such that they produced smaller SO_2 emissions. Low acoustic energies observed from Events 16–18, relative to Events 2–6, as described by Fee et al. (2013) are consistent with (2) as acoustic energies have shown broad correlation with gas emissions (Dalton et al., 2010; Fee et al., 2013).

High variability in daily SO_2 mass emissions during the effusive phase of the eruption from below detection limit to ~24.6 kt (12 April; Fig. 6) make relationships between degassing and volcanic activity difficult to constrain during this period. Evidence from satellite imagery, time-lapse photography, and photogrammetry of dome growth was consistent throughout this period (Bull and Buurman, 2013; Diefenbach et al., 2013), and thus degassing of extruding lava can explain the moderate level emissions. We propose that variations in daily OMI measured SO_2 masses throughout this period may be due to a variety of factors including both variations in volcanic and instrument retrieval factors. Specifically, changes in lava composition, vesicularities, and/or extrusion rates could produce changes in SO_2 emission rates. For example, high SO_2 emissions observed by OMI from 4 to 6 May correlate with increased extrusion rates (Diefenbach et al., 2013), variations in lava composition (Coombs et al., 2013), elevated seismicity (Buurman et al., 2013), and an increase in airborne gas emissions (Werner et al., 2013) all of which support a change in the volcanic system. Other periods of elevated OMI measured SO_2 emissions during the sample period include 8–12 and 18–20 April, which also could be attributed to changing magmatic conditions, however more corroborating evidence is required to develop this hypothesis. Additionally, it is probable that variations in OMI viewing conditions, atmospheric composition, and surface reflectivity may cause apparent variations in SO_2 emission rates (Yang et al., 2007). While clear divisions between levels of SO_2 emissions for different types of volcanic activity were apparent during the

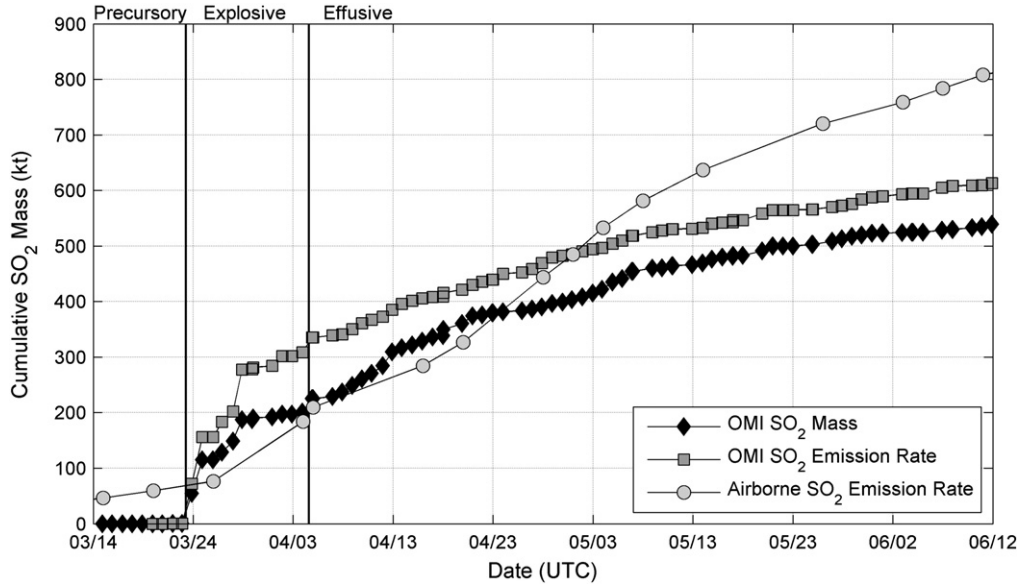

Fig. 8. Cumulative SO_2 masses emitted from Redoubt Volcano as estimated from OMI daily mass (black triangles), OMI-derived emission rate (gray squares), and airborne methods (light gray circles). The black vertical lines represent the temporal breaks between precursory (left), explosive (center), and effusive (right) phases of the eruption. Note that airborne measurements from the two months preceding the first OMI detection of Mount Redoubt SO_2, of ~46 kt are included in this figure.

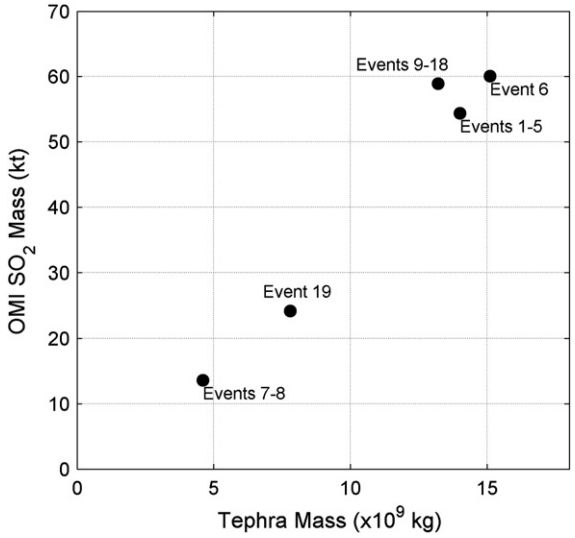

Fig. 9. Comparison between SO_2 and tephra masses for Mount Redoubt's explosive events. A strong ($R^2 = 0.97$) linear correlation can be seen.
Tephra masses from Wallace et al. (2013).

explosive phase of the eruption, these same divisions did not apply to the effusive phase SO_2 emissions. These results suggest that for times corresponding with known explosive eruptions, OMI daily SO_2 masses can be used to infer relative eruption size and explosivity. For other times, OMI daily SO_2 masses may be used to help distinguish explosive from extrusive degassing, and may help resolve variations in lava extrusion rates when used in conjunction with other observational datasets.

5.8. Apparent periodicity in OMI measured SO_2 masses

An apparent periodicity is visible within the OMI daily SO_2 masses throughout the study period (Fig. 10). To evaluate the periodicity as a function of time a 12–18 day filter was applied to the SO_2 masses during the study period (Fig. 10, top) using a 2-pole, acausal, butterworth filter (Hayes, 1996). A clear periodic trend can be seen in the filtered data throughout the sample period. To better constrain the dominant period in the data a Power Spectral Density (PSD) estimate was made using Welch's modified periodogram method (Hayes, 1996) (Fig. 10, bottom). This method is chosen as it reduces the noise in the power spectra by dividing the data into overlapping segments and then averaging the power spectra. Two dominant periods of approximately 4 and 16 days within the OMI daily SO_2 mass dataset exist (Fig. 10, bottom), though high uncertainties are present due to the limited number of samples (85 days). Several scenarios could explain the periodicities including, but not limited to: (1) changes in OMI viewing geometry; (2) changes in the atmospheric composition and conditions, specifically with respect to ozone and cloud cover (e.g. Prata, 1990); (3) changes within the volcanic system itself such as variations in lava extrusion rate, magma convection and/or ascent, conduit permeability, etc. (Andres et al., 1993; Edmonds et al., 2003; Sutton et al., 2003); and (4) tidal stresses (e.g. Sottili et al., 2007). The PSD methods described above were applied to daily earthquake number at Redoubt Volcano for the study period and no dominant period was found, supporting a non-volcanic source to the periodicity. OMI has a 16 day or 233 orbit repeat cycle, meaning that OMI's orbital viewing geometry repeats every 16 days or 233 orbits. Certain orbital viewing geometries (e.g. near-nadir overpasses) are more favorable for detection of SO_2 from Redoubt Volcano, which likely contributes to the apparent 16 day periodicity observed within the OMI daily SO_2 mass dataset. This has implications for monitoring SO_2 emissions with OMI, as changes in measured daily SO_2 masses could be due to either changes in SO_2 production (e.g. volcanic activity or anthropogenic sources), changes in OMI viewing geometries, or both. Future work should be conducted to constrain possible influences by other non-volcanic sources and to evaluate the affect of OMI viewing geometries on measured SO_2 masses.

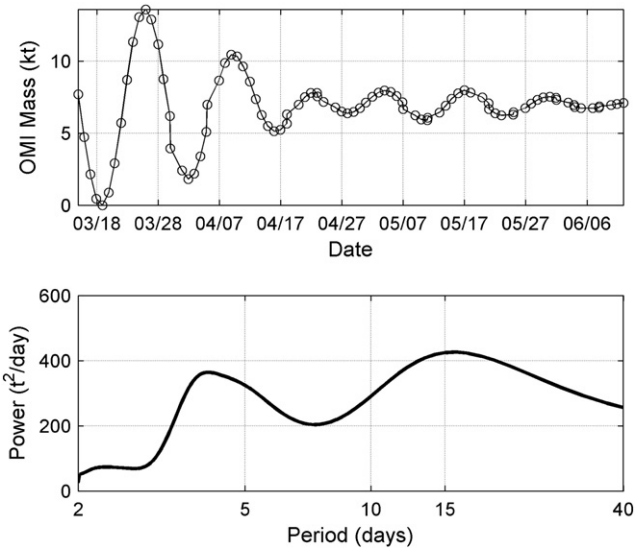

Fig. 10. OMI daily measured SO_2 mass data filtered between 12 and 18 days (top) and Power Spectral Density analysis on the 85 day dataset, showing apparent dominant periodicities at ~4 and 16 days (bottom).

5.9. Evaluation of OMI as a volcano monitoring tool

The results of this study show that OMI was a useful tool for monitoring Mount Redoubt's volcanic SO_2 emissions during the 2009 eruption, and emphasize the utility of OMI as a volcano monitoring technology. Significant advantages in using OMI to monitor SO_2 emissions relative to traditional airborne methods or other satellite sensors include: (1) the ability to detect SO_2 emissions during explosive activity when it may not be safe or feasible to collect airborne measurements; (2) OMI's sensitivity to SO_2, allowing both low altitude (<3 km) and relatively weak (~2000 t/d SO_2) plumes to be detected, as this type of plume often goes undetected by other satellite sensors; (3) the relatively high temporal resolution of OMI data, one or more measurement per day compared to weekly or biweekly airborne measurements; and (4) the affordability of measurement collection as the data are freely available and only require analyst time for image processing and interpretation. Additionally, we have shown that OMI-derived emission rates agree well with airborne measurements, such that OMI data can be successfully integrated into airborne databases. OMI's ability to detect SO_2 from Redoubt Volcano on a near daily basis make it possible for gas data to be used in conjunction with other high temporal resolution geophysical datasets to help detect changes in volcanic activity and improve AVO's monitoring capabilities, especially for remote Alaskan volcanoes.

6. Conclusions

OMI detected SO_2 emissions from Redoubt Volcano on 67 out of 82 days analyzed between 23 March (the onset of the explosive eruption) and 12 June 2009. Comparison between OMI and corrected airborne SO_2 CD values show that in general for Mount Redoubt's ~3 km plume, the OMI *TRL* altitude algorithm underestimated, while the *PBL* altitude algorithm overestimated SO_2 CD. Good ($R^2 = 0.75$) and poor ($R^2 = 0.38$) correlations between OMI and corrected airborne CD values were observed for the *PBL* and *TRL* altitude algorithms, respectively. OMI daily SO_2 masses for the study period ranged from

~60.1 kt on 24 March to below detection limit, with an average daily SO_2 mass emitted during the study period of ~6.7 kt. The highest quantity SO_2 emissions were observed during the initial part of the explosive phase and the emissions exhibited an overall decreasing trend with time, though some periods of higher emissions were observed. OMI SO_2 emission rates were calculated using three methods and compared to airborne measurements. Results of this comparison found good agreement ($R^2 = 0.82$) between OMI *Method 1* derived and airborne emission rates, with OMI underestimating SO_2 relative to airborne measurements in most cases. The comparison between OMI and airborne calculated emission rates suggests that OMI's detection limit for high latitude, springtime conditions is between 2000 and 4000 t/d and may improve with increasing UV radiation, though further comparisons are needed to corroborate this. Cumulative SO_2 masses calculated from OMI daily mass and derived emission rates for the study period are estimated to range from 542 to 615 kt, with approximately half of the cumulative SO_2 having been erupted during the explosive phase of the eruption. These values are similar in magnitude to those estimated for the 1989–90 Mount Redoubt eruption.

The relatively high temporal resolution OMI dataset allowed comparisons with other observational datasets and find strong correlations between OMI daily SO_2 mass and both relative acoustic energy and tephra mass during the explosive phase of the 2009 Mount Redoubt eruption, suggesting that OMI data may be used to infer relative eruption explosivity and size associated with known explosive eruptions. Further, when used in conjunction with other geophysical and geochemical datasets OMI daily SO_2 masses may be used to help distinguish explosive from effusive activity and detect changes in lava extrusion rates. The results of this study find that OMI is a useful volcano monitoring tool to complement airborne measurements, capture explosive SO_2 emissions, identify potentially hazardous volcanic clouds, and provide high temporal resolution SO_2 emissions data that can be used with complementary datasets to elucidate volcanic processes.

Supplementary materials related to this article can be found online at doi:10.1016/j.jvolgeores.2012.03.002.

Acknowledgments

The authors are grateful for constructive comments by Chris Waythomas and two anonymous reviewers whose suggestions significantly improved this manuscript. The authors would like to acknowledge pilots Steve Jones and Jerry Morris from Security Aviation as well as AVO scientists Rick Wessels, Game McGimsey and Tina Neal, for their contributions to airborne gas measurement collection. TML would like to thank Kate Bull, Helena Buurman, Ronni Grapenthin, Michelle Coombs, Jon Dehn, Bill Simpson, Rainer Newberry, Owen Neill, Sarah Henton and Trystan Herriott for insightful scientific discussions regarding this work. TML would like to thank Angela Ekstrand for help with figure creation and Helena Buurman for providing daily earthquake data for PSD analysis. SAC acknowledges NASA funding for OMI SO_2 validation (grant NNX09AJ40G). This work has been funded by the Alaska Volcano Observatory, the UAF Geophysical Institute, the Alaska Space Grant Consortium, and the American Recovery and Reinvestment Act (ARRA) grant.

References

Andres, R.J., Rose, W.I., Stoiber, R.E., Williams, S.N., Matias, O., Morales, R., 1993. A summary of sulfur dioxide emission rate measurements from Guatemalan volcanoes. Bulletin of Volcanology 55, 379–388. doi:10.1007/BF00301150.

Blake, S., 2003. Correlations between eruption magnitude, SO_2 yield, and surface cooling. In: Oppenheimer, C., Pyle, D., Barclay, J. (Eds.), Volcanic Degassing. Geological Society, London, pp. 371–380.

Bleick, H.A., Coombs, M.L., Cervelli, P.F., Bull, K.F., Wessels, R.L., 2013. Volcano–ice interactions precursory to the 2009 eruption of Redoubt Volcano, Alaska. Journal of Volcanology and Geothermal Research 259, 373–388.

Bluth, G., Carn, S., 2008. Exceptional sulfur degassing from Nyamuragira volcano, 1979–2005. International Journal of Remote Sensing 29 (22), 6667–6685. doi:10.1080/01431160802168434.

Bluth, G.J.S., Schnetzler, C.C., Krueger, A.J., Walter, L.S., 1993. The contribution of explosive volcanism to global atmospheric sulphur dioxide concentrations. Nature 366, 327–329. doi:10.1080/01431160802168434.

Bull, K.F., Buurman, H., 2013. An overview of the 2009 eruption of Redoubt Volcano, Alaska. Journal of Volcanology and Geothermal Research 259, 2–15.

Buurman, H., West, M.E., Thompson, G., 2013. The seismicity of the 2009 Redoubt eruption. Journal of Volcanology and Geothermal Research 259, 16–30.

Carn, S., 2011. OMIplot Software. http://vhub.org/resources/6822011.

Carn, S.A., Lopez, T.M., 2011. Opportunistic validation of sulfur dioxide in the Sarychev Peak volcanic eruption cloud. Atmospheric Measurement Techniques 4, 1705–1712. doi:10.5194/amt-4-1705-2011.

Carn, S.A., Strow, L.L., de Souza-Machado, S., Edmonds, Y., Hannon, S., 2005. Quantifying tropospheric volcanic emissions with AIRS: the 2002 eruption of Mt. Etna (Italy). Geophysical Research Letters 32 (2), L02301. doi:10.1029/2004gl021034.

Carn, S., Krueger, A., Krotkov, N., Yang, K., Levelt, P., 2007. Sulfur dioxide emissions from Peruvian copper smelters detected by the Ozone Monitoring Instrument. Geophysical Research Letters 34, L09801. doi:10.1029/2006GL029020.

Carn, S.A., Krueger, A.J., Arellano, S., Krotkov, N.A., Yang, K., 2008a. Daily monitoring of Ecuadorian volcanic degassing from space. Journal of Volcanology and Geothermal Research 176, 141–150. doi:10.1016/j.jvolgeores.2008.01.029.

Carn, S.A., Prata, A.J., Karlsdóttir, S., 2008b. Circumpolar transport of a volcanic cloud from Hekla (Iceland). Journal of Geophysical Research 113 (D14), D14311. doi:10.1029/2008jd009878.

Carn, S., Krueger, A., Krotkov, N., Yang, K., Evans, K., 2009. Tracking volcanic sulfur dioxide clouds for aviation hazard mitigation. Natural Hazards 51 (2), 325–343. doi:10.1007/s11069-008-9228-4.

Carn, S.A., Froyd, K.D., Anderson, B.E., Wennberg, P., Crounse, J., Spencer, K., Dibb, J.E., Krotkov, N.A., Browell, E.V., Hair, J.W., Diskin, G., Sachse, G., Vay, S.A., 2011. In situ measurements of tropospheric volcanic plumes in Ecuador and Colombia during TC^4. Journal of Geophysical Research — Atmosphere 116, DOOJ24. doi:10.1029/2010JD014718.

Casadevall, T., Doukas, M., Neal, C., McGimsey, G., Gardner, C., 1994. Emision rates of sulfur dioxide and carbon dioxide from Redoubt Volcano, Alaska during the 1989–1990 eruptions. Journal of Volcanology and Geothermal Research 62, 519–530. doi:10.1016/0377-0273(94)90050-7.

Coombs, M.L., Sisson, T.W., Bleick, H.A., Henton, S.M., Nye, C.J., Payne, A.L., Cameron, C.E., Larsen, J.F., Wallace, K.L., Bull, K.F., 2013. Andesites of the 2009 eruption of Redoubt Volcano, Alaska. Journal of Volcanology and Geothermal Research 259, 349–372.

Daag, A., Tubianosa, B., Newhall, C., Tungol, N., Javier, D., Dolan, M., Delos-Reyese, P., Arboleda, R., Martinez, M., Regalado, T., 1996. Monitoring sulfur dioxide emissions at Mount Pinatubo. In: Newhall, C., Punongbayan, R. (Eds.), Fire and Mud: Eruptions and Lahars of Mount Pinatubo, Philippines. University of Washington, Seattle, pp. 409–414.

Dalton, M., Waite, G., Watson, I., Nadeau, P., 2010. Multiparameter quantification of gas release during weak Strombolian eruptions at Pacaya Volcano, Guatemala. Geophysical Research Letters 37, L09303. doi:10.0129/2010g1042617.

Diefenbach, A.K., Bull, K.F., Wessels, R.L., McGimsey, R.G., 2013. Photogrammetric monitoring of lava dome growth during the 2009 eruption of Redoubt Volcano. Journal of Volcanology and Geothermal Research 259, 308–316.

Doukas, M., 1995. A compilation of sulfur dioxide and carbon dioxide emissions-rate data from Cook Inlet volcanoes (Redoubt, Spurr, Iliamna, and Augustine), Alaska during the period from 1990–1994. U.S. Geological Survey. Open-File Report 95-0055.

Doukas, M., 2002. A new method for GPS-based wind speed determineations during airborne volcanic plume measurements. U.S. Geological Survey Open-File Report 02-395.

Doukas, M., Gerlach, T., 1995. Sulfur dioxide scrubbing during the 1992 eruption of Crater Peak, Spurr Volcano, Alaska. In: Keith, T. (Ed.), The 1992 Eruption of Crater Peak Vent, Mount Spurr Volcano, Alaska. U.S. Geological Survey, Washington.

Doukas, M., McGee, K., 2007. A compilation of gas emission-rate data from volcanoes of Cook Inlet (Spurr, Crater Peak, Redoubt, Illiamna, and Augustine) and Alaska Peninsula (Douglas, Fourpeaked, Griggs, Mageik, Martin, Peulik, Ukinrek Maars, and Veniaminof), Alaska, from 1995–2006. U.S. Geological Survey Open File Report 07-1400.

Edmonds, M., Oppenheimer, C., Pyle, D., Herd, R., Thompson, G., 2003. SO_2 emissions from Soufriere Hills Volcano and their relationship to conduit permeability, hydrothermal interaction and degassing regime. Journal of Volcanology and Geothermal Research 124, 23–43. doi:10.1016/S0377-0273(03)00041-6.

Fee, D., Garces, M., Steffke, A., 2010. Infrasound from Tungurahua Volcano 2006–2008: Strombolian to Plinian eruptive activity. Journal of Volcanology and Geothermal Research 193, 67–81. doi:10.1016/j.jvolgeores.2010.03.006.

Fee, D., McNutt, S.R., Lopez, T.M., Arnoult, K.M., Szuberla, C.A.L., Olson, J.V., 2013. Combining local and remote infrasound recordings from the 2009 Redoubt Volcano eruption. Journal of Volcanology and Geothermal Research 259, 100–114.

Fischer, T., Arehart, G., Sturchio, N., Williams, S., 1996. The relationship between fumarole gas composition and eruptive activity at Galeras Volcano, Colombia. Geology 24 (6), 531–534. doi:10.1130/0091-7613(1996) 024<0531:TRBFGC>2.3.CO;2.

Gerlach, T., 2003. Elevation effects in volcano applications of the COSPEC. In: Oppenheimer, C., Pyle, D., Barclay, J. (Eds.), Volcanic Degassing. The Geological Society of London, London, pp. 169–175.

Gerlach, T., Delgado, H., McGee, K., Doukas, M., Venegas, J., Cardenas, L., 1997. Application of the LI-COR CO_2 analyzer to volcanic plumes: a case study, volcan Popocateptetl, Mexico, June 7 and 10, 1995. Journal of Geophysical Research 102 (B4), 8005–8019. doi:10.1029/96JB03887.

Grapenthin, R., Freymueller, J.T., Kaufman, A.M., 2013. Geodetic observations during the 2009 eruption of Redoubt Volcano, Alaska. Journal of Volcanology and Geothermal Research 259, 115–132.

Hayes, M., 1996. Statistical Digital Signal Processing and Modeling. John Wiley & Sons.

Hobbs, P., Radke, L., Lyons, J., Ferek, R., Coffman, D., Casadevall, T., 1991. Airborne measurements of particle and gas emissions from the 1990 volcanic eruption of Mount Redoubt. Journal of Geophysical Research 96 (D10), 18,735–18,752.

Hotovec, A.J., Prejean, S.G., Vidale, J.E., Gomberg, J., 2013. Strongly gliding harmonic tremor during the 2009 eruption of Redoubt Volcano. Journal of Volcanology and Geothermal Research 259, 89–99.

Kelly, P.J., Kern, C., Roberts, T.J., Lopez, T., Werner, C., Aiuppa, A., 2013. Rapid chemical evolution of tropospheric volcanic emissions from Redoubt Volcano, Alaska, based on observations of ozone and halogen-containing gases. Journal of Volcanology and Geothermal Research 259, 317–333.

Kern, C., Deutschmann, T., Vogel, L., Wohrbach, M., Wagner, T., Platt, U., 2010. Radiative transfer corrections for accurate spectroscopic measurements of volcanic gas emissions. Bulletin of Volcanology 72 (2), 233–247. doi:10.1007/s00445-009-0313-7.

Krotkov, N., Carn, S., Krueger, A., Bhartia, P., Yang, K., 2006. Band residual difference algorithm for retrieval of SO_2 from the Aura Ozone Monitoring Instrument. IEEE Transactions on Geoscience and Remote Sensing 44 (5), 1259–1266. doi:10.1109/TGRS.2005.861932.

Krotkov, N., McClure, B., Dickerson, R., Carn, S., Li, C., Bhartia, P., Yang, K., Krueger, A., Li, Z., Levelt, P., Chen, H., Wang, P., Lu, D., 2008. Validation of SO_2 retreivals from the Ozone Monitoring Instrument over NE China. Journal of Geophysical Research 113. doi:10.1029/2007JD008818.

Kurosu, T., Celarier, E., 2010. OMPIXCOR Readme File. http://disc.sci.gsfc.nasa.gov/Aura/data-holdings/OMI/documents/v003/OMPIXCOR_README_V003.pdf2010.

Levelt, P.F., Hilsenrath, E., Leppelmeier, G.W., van den Oord, G.H.J., Bhartia, P.K., Tamminen, J., de Haan, J.F., Veefkind, J.P., 2006. Science objectives of the ozone monitoring instrument. IEEE Transactions on Geoscience and Remote Sensing 44 (5), 1199–1208. doi:10.1109/TGRS.2006.872336.

McGee, K., Doukas, M., McGimsey, G., Neal, C., Wessels, R., 2010. Emission of SO_2, CO_2, and H_2S from Augustine Volcano, 2002–2008. In: Power, J., Coombs, M., Freymueller, J. (Eds.), The 2006 Eruption of Augustine Volcano, Alaska. U.S. Geological Survey, pp. 609–627.

Neal, C.A., Murray, T.L., Power, J.A., Adleman, J.N., Whitmore, P.M., Osiensky, J.M., 2010. Hazard information management, interagency coordination, and impacts of the 2005–2006 eruption of Augustine volcano. In: Power, J.A., Coombs, M.L., Freymueller, J.T. (Eds.), The 2006 Eruption of Augustine Volcano, Alaska. U.S. Geological Survey, pp. 645–667.

Oppenheimer, C., Francis, P., Stix, J., 1998. Depletion rates of sulfur dioxide in tropospheric volcanic plumes. Geophysical Research Letters 25 (14), 2671–2674. doi:10.1029/98GL01988.

Pfeffer, M., Langmann, B., Graf, H.-F., 2006. Atmospheric transport and deposition of Indonesian volcanic emissions. Atmospheric Chemistry and Physics 6, 2525–2537.

Platt, U., Stutz, J., 2008. Differential Optical Absorption Spectroscopy Principles and Applications. Springer-Verlag, Berlin–Heidelberg, pp. 137–141.

Prata, A., 1990. Travelling waves in Nimbus-7 SBUV ozone measurements: observations and theory. Quarterly Journal of the Royal Meteorological Society 116, 1091–1122. doi:10.1002/qj.49711649505.

Prata, A., Bernardo, C., 2007. Retrieval of volcanic SO_2 column abundance from Atmospheric Infrared Sounder data. Journal of Geophysical Research 112. doi:10.1029/2006JD007955.

Rodriguez, L., Watson, I., Edmonds, M., Ryan, G., Hards, V., Oppenheimer, C., Bluth, G., 2008. SO_2 loss rates in the plume emitted by Soufriere Hills volcano, Montserrat. Journal of Volcanology and Geothermal Research 173, 135–147. doi:10.1016/j.jvolgeores.2008.01.003.

Rybin, A., Chibisova, M., Webley, P., Steesen, T., Izbekov, P., Neal, C., Realmuto, V., 2011. Satellite and ground observations of the June 2009 eruption of Sarychev Peak volcano, Matua Island, Central Kuriles. Bulletin of Volcanology 73 (9), 1377–1392. doi:10.1007/s00445-011-0481-0.

Schaefer, J., Cameron, C., Nye, C., 2009. Historically active volcanoes of Alaska. Alaska Division of Geological and Geophysical Surveys Miscellaneous Publication, 133. http://www.dggs.dnr.state.ak.us/pubs/pubs?reqtype=citation&ID=20181.

Schaefer, J., Bull, K.F., Cameron, C., Coombs, M., Diefenbach, A.K., Lopez, T., McNutt, S., Neal, C., Payne, A., Power, J., Schneider, D., Scott, W., Snedigar, S., Thompson, G., Wallace, K., Waythomas, C., Webley, P., Werner, C., 2012. The 2009 eruption of Redoubt Volcano, Alaska. Alaska Division of Geological and Geophysical Surveys Report of Investigations, 2011-5, p. 45.

Schneider, D.J., Hoblitt, R.P., 2013. Doppler weather radar observations of the 2009 eruption of Redoubt Volcano, Alaska. Journal of Volcanology and Geothermal Research 259, 133–144.

Schnetzler, C., Doiron, S., Walter, L., Krueger, A., 1994. Satellite measurement of sulfur dioxide from the Redoubt eruptions of 1989–1990. Journal of Volcanology and Geothermal Research 62, 353–357. doi:10.1016/0377-0273(94)90041-8.

Sottili, G., Martino, S., Palladino, D.M., Paciello, A., Bozzano, F., 2007. Effects of tidal stresses on volcanic activity at Mount Etna, Italy. Geophysical Research Letters 34, L01311. doi:10.0129/2006GL028190,2007.

Spinei, E., Carn, S., Krotkov, N., Mount, G., Yang, K., Krueger, A., 2010. Validation of ozone monitoring instrument SO_2 measurements in the Okmok volcanic cloud over Pullman, WA, July 2008. Journal of Geophysical Research 115, D00L08. doi:10.1029/2009JDO13492,2010.

Stoiber, R., Malinconico, L., Williams, S., 1983. The use of correlation spectrometers at volcanoes. In: Tazieff, H., Sabroux, J. (Eds.), Forecasting Volcanic Events. El Sevier, Amsterdam–New York, pp. 425–444.

Surono, P., Jousset, P., Pallister, J., Boichu, M., Buongiorno, M.F., Budisantoso, A., Costa, F., Andreastuti, S., Prata, F., Schneider, D., Clarisse, L., Humaida, H., Sumarti, S., Bignami, C., Griswold, J., Carn, S., Oppenheimer, C., Lavigne, F., 2012. The 2010 explosive eruption of Java's Merapi volcano — A '100-year' event. Journal of Volcanology and Geothermal Research 241–242, 121–135.

Sutton, A.J., Elias, T. and Kauahikaua, J., 2003. Lava-effusion rates for the Pu'u O'o-Kupaianaha eruption derived from SO_2 emissions and very low frequency measurements. In: U.S.G. Survey (Editor), The Pu'u O'o-Kupaianaha Eruption of Kilauea Volcano, Hawai'i: The First 20 Years, pp. 137–148.

Symonds, R.B., Gerlach, T.M., Reed, M.H., 2001. Magmatic gas scrubbing: implications for volcano monitoring. Journal of Volcanology and Geothermal Research 108 (1–4), 303–341. doi:10.1016/S0377-0273(00)00292-4.

Thomas, H., Prata, A., 2011. Sulphur dioxide as a volcanic ash proxy during the April–May 2010 eruption of Eyjafjallajokull Volcano, Iceland. Atmospheric Chemistry and Physics 11, 6871–6880. doi:10.5194/acp-11-6871-2011.

Thomas, H., Watson, I., 2009. Observations of volcanic emissions from space: current and future perspectives. Natural Hazards 54 (2), 323–354. doi:10.1007/s11069-009-9471-3.

Thomas, H., Watson, I., Kearney, C., Carn, S., Murray, S., 2009. A multi-sensor comparison of sulphur dioxide emissions from the 2005 eruption of Sierra Negra volcano, Galapagos Islands. Remote Sensing of Environment 113, 1331–1342. doi:10.1016/j.rse.2009.02.019.

Wallace, K.L., Schaefer, J.R., Coombs, M.L., 2013. Character,mass, distribution, and origin of tephra-fall deposits from the 2009 eruption of Redoubt Volcano, Alaska—Highlighting the significance of particle aggregation. Journal of Volcanology and Geothermal Research 259, 145–169.

Webley, P.W., Lopez, T.M., Ekstrand, A.L., Dean, K.G., Rinkleff, P., Dehn, J., Cahill, C.F., Wessels, R.L., Bailey, J.E., Izbekov, P., Worden, A., 2013. Remote observations of eruptive clouds and surface thermal activity during the 2009 eruption of Redoubt volcano. Journal of Volcanology and Geothermal Research 259, 185–200.

Werner, C., Doukas, M., Kelly, P., 2011. Gas emissions from failed and actual eruptions from Cook Inlet Volcanoes, Alaska, 1989–2006. Bulletin of Volcanology 73, 155–173. doi:10.0117/s00445-011-0453-4.

Werner, C., Kelly, P.J., Doukas, M., Lopez, T., Pfeffer, M., McGimsey, R., Neal, C., 2013. Degassing of CO2, SO2, and H_2S associated with the 2009 eruption of Redoubt Volcano, Alaska. Journal of Volcanology and Geothermal Research 259, 270–284.

Williams-Jones, G., Stix, J., Nadeau, P., 2008. Using the COSPEC in the field. In: Williams-Jones, G., Stix, J., Hickson, C. (Eds.), The COSPEC Cookbook: Making SO_2 Measurements at Active Voclanoes. IAVCEI, pp. 63–119.

Yang, K., Krotkov, N., Krueger, A., Carn, S., Bhartia, P., Levelt, P., 2007. Retrieval of large volcanic SO_2 columns from the Aura Ozone Monitoring Instrument: comparison and limitations. Journal of Geophysical Research 112, D24S43. doi:10.1029/2007JD008825.